A volcanotectonic survey of Ascraeus Mons, Mars

Paul K. Byrne,[1,2,3] Benjamin van Wyk de Vries,[2] John B. Murray,[4] and Valentin R. Troll[1,5]

Received 3 March 2011; revised 17 October 2011; accepted 26 October 2011; published 18 January 2012.

[1] Ascraeus Mons is one of the largest volcanoes on Mars. It is replete with well-preserved features that can be used to understand its volcanotectonic evolution. Previous studies of this volcano focused on specific features, and were limited by the quality and coverage of contemporary data. Our objective is to review and enhance the existing developmental model for Ascraeus by considering all endogenic surface features on the volcano. We surveyed the volcano's caldera complex, flank terraces, pit structures, sinuous rilles, arcuate grabens, and small vents. We report the spatial and temporal distributions of these features, appraise their proposed formation mechanisms in light of our mapping results, and propose a detailed geological history for Ascraeus Mons. An initial shield-building phase was followed by the formation of a summit caldera complex and small parasitic cones, while compression due to flexure of the supporting basement led to extensive terracing of the shield flanks. An eruptive hiatus followed, ending with the construction of expansive rift aprons to the northeast and southwest. Against later, extensive flank resurfacing in the late Amazonian, continued flexure formed arcuate grabens concentric to the edifice. Localized eruption and surface flow of a fluid agent (lava and/or water) from within the volcano then produced a population of rilles on the lower flanks. Finally, in a change of flank tectonic regime from compression to extension, pit crater chains and troughs developed on the main shield and rift aprons, eventually coalescing to form large embayments at the northeast and southwest base of the volcano.

Citation: Byrne, P. K., B. van Wyk de Vries, J. B. Murray, and V. R. Troll (2012), A volcanotectonic survey of Ascraeus Mons, Mars, *J. Geophys. Res.*, *117*, E01004, doi:10.1029/2011JE003825.

1. Introduction

[2] The Tharsis Rise is an expansive plateau that straddles the western hemisphere of Mars, and is the location of some of the planet's most recent and extensive volcanism [*Hodges and Moore*, 1994]. It is host to swarms of monogenetic cones [*Hughes et al.*, 2008; *Baratoux et al.*, 2009; *Hauber et al.*, 2009] and several giant volcanoes, of which Olympus Mons is the tallest [*Plescia*, 2004]. To the north, the Rise is dominated by three enormous shields, known collectively as the Tharsis Montes, aligned along a northeast-southwest oriented topographic high [*Carr et al.*, 1977]. Arsia Mons is the southernmost Tharsis volcano, and with a vertical relief of 11.7 km is over 3,000 m taller than is its neighbor, Pavonis Mons. To the northeast, this triad is completed by the tallest and youngest Tharsis shield, Ascraeus Mons (Figure 1, inset).

[3] Ascraeus has an array of prominent, well-preserved structural and morphological features, including a summit caldera complex, pit craters, and sinuous rilles, which provides information on Martian volcano and mantle dynamics, and which has served as a framework for much of our understanding of the volcanotectonic history of the Tharsis volcanoes [*Crumpler and Aubele*, 1978; *Crumpler et al.*, 1996; *Scott and Wilson*, 1999, 2000; *Wyrick et al.*, 2004; *Bleacher et al.*, 2007a; *Murray et al.*, 2010]. Descriptions of additional features on this volcano, such as flank terraces [*Thomas et al.*, 1990], load-concentric arcuate grabens, and small vents, have been hampered in the past by the lack of photogeological data of sufficiently high resolution for detailed mapping, however, and so have been overlooked when investigating this and other volcanoes' histories. With the recent availability of such data [e.g., *Byrne et al.*, 2009], the opportunity now exists to examine all feature types on Ascraeus, and to test existing models for its volcanological and structural development.

[4] In this study, we use High Resolution Stereo Camera (HRSC) images, supplemented by Context Imager (CTX) data, together with the Mars Orbiter Laser Altimeter (MOLA) gridded data set within a Geographical Information System (GIS) to survey the volcano's most prominent surface features (described in section 2.1). We report the spatial and temporal distributions of these features, review their proposed formation mechanisms in light of our mapping

[1]Department of Geology, Trinity College Dublin, Dublin, Ireland.
[2]Laboratoire Magmas et Volcans, Université Blaise-Pascal, Clermont-Ferrand, France.
[3]Now at Department of Terrestrial Magnetism, Carnegie Institution of Washington, Washington, D. C., USA.
[4]Department of Earth Sciences, Open University, Milton Keynes, UK.
[5]Now at Department of Earth Sciences, Uppsala University, Uppsala, Sweden.

0148-0227/12/2011JE003825

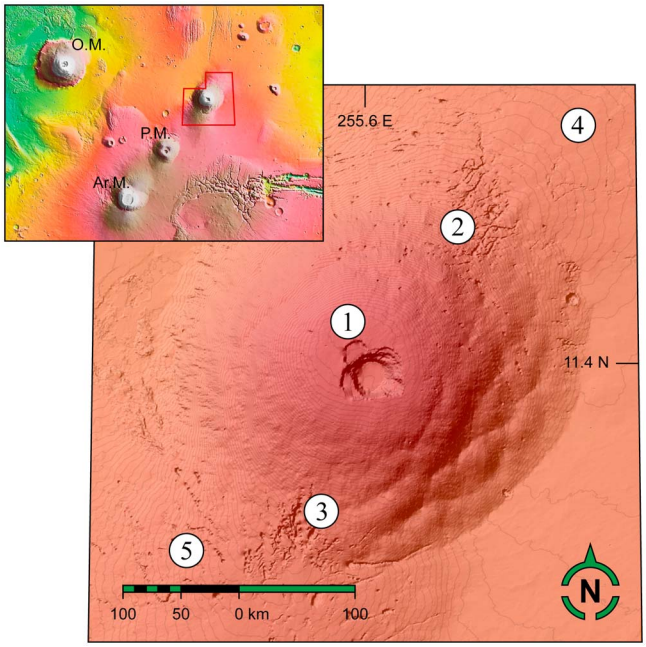

Figure 1. MOLA-derived hillshade map of Ascraeus Mons, illuminated from the northwest. Key morphological features of the volcano are shown: the planar summit (1), which hosts the caldera complex; the northeast (2) and southwest (3) flank embayments; and the northeast- (4) and southwest- (5) trending rift aprons. The map is displayed with contours at 1,000 m intervals and with a sinusoidal projection. The longitude value given here and in each subsequent figure is relative to a coordinate system with an east positive center of longitude. Inset: a portion of the global MOLA elevation map, showing the location of Ascraeus Mons (outlined) with respect to Arsia Mons (Ar.M.), Pavonis Mons (P.M.), and Olympus Mons (O.M.). Inset image credit: JPL/NASA.2845103.

results, and integrate our results with the current accepted paradigm for the geological history of Ascraeus Mons.

2. Ascraeus Mons

[5] Ascraeus is the third-largest volcano on Mars, with a volume of 1.1×10^6 km^3 and a vertical relief of 14,900 m [*Plescia*, 2004]. Like its Tharsis counterparts, Ascraeus has a convex-upward morphology, a summit plateau and caldera complex (Figure 1: 1), and substantial erosional features ("embayments") on the northeast and southwest flanks (Figure 1: 2, 3), from which extensive overlapping lavas emanate ("rift aprons") (Figure 1: 4, 5) [*Hodges and Moore*, 1994]. The southwest embayment, termed the Ascraeus Chasmata [*Murray et al.*, 2010], is particularly extensive, measuring 55 km east-west and 75 km north-south (Figure 1: 3). While generally classified as shield volcanoes [*Carr et al.*, 1977; *Scott and Tanaka*, 1986; *Hodges and Moore*, 1994], *Head and Wilson* [1998] suggested that the Tharsis Montes be regarded as stratovolcanoes based on edifice morphology and the likelihood of explosive eruptions during the early phases of their growth.

[6] Long, ribbon-like flows, primarily sourced from flank eruptions [*Mouginis-Mark*, 1981] and characteristic of large Martian shields [*Plescia and Saunders*, 1979], are evident on the main flanks of Ascraeus. Recent high-resolution photogeological mapping of Ascraeus indicates a transition from tube- to channel-fed eruption conditions on the main flanks, with a prevalence of tube-fed eruptions on the rift aprons [*Bleacher et al.*, 2007a, 2007b]. *Hiesinger et al.* [2007] used a flow model with data derived from photogeological mapping to calculate values for the mean viscosity and average effusion rate of lavas on the main portion of the volcano, yielding values of $\sim 4.1 \times 10^6$ Pa.s and 185 m^3.s^{-1}, respectively.

[7] The northeast lava apron is larger than that to the southwest [*Plescia*, 2004], while the latter overprints the northeastern apron of nearby Pavonis [*Hodges and Moore*, 1994]. Though commonly regarded as being exclusively composed of lava flows, *Murray et al.* [2010] suggested that portions of the rift aprons consist of mudflows and lahars, the result of material deposited at the base of volcano by groundwater issuing from its flanks.

[8] Aureole deposits, similar to those observed at Olympus, Pavonis, and Arsia (although more areally restricted at the latter two), occur at the northwest base of Ascraeus, on the topographic downslope of the Tharsis Rise [*Zimbelman and Edgett*, 1992]. Proposed formation mechanisms for the deposits surrounding Olympus, which include gravity spreading [*Lopes et al.*, 1980; *Francis and Wadge*, 1983; *Tanaka*, 1985; *McGovern et al.*, 2004; *McGovern and Morgan*, 2005, 2009], ash flow deposition [*Morris*, 1982], erosion of sub-glacial eruptives [*Hodges and Moore*, 1979, 1994], or gravity-induced thrusting [*Harris*, 1977], could also be directly applicable to Ascraeus Mons. Upslope of these deposits, the northwest flank shows extensive scalloped and pitted textures.

[9] On the basis of volcano morphology and crater frequency-diameter distributions, *Crumpler and Aubele* [1978] proposed an evolutionary sequence for the Tharsis Montes, comprising (1) the development of a main shield through the accumulation of thick lava plains, (2) summit subsidence and the formation of concentric fractures and grabens due to magma chamber evacuation, possibly caused by the outbreak of parasitic eruption centers on the northeast and southwest flanks, and (3) the formation of the large rift aprons to the northeast and southwest as volcanism continued from these lower eruption centers. These authors suggested that Arsia Mons represents the final stage of this sequence, and Pavonis and Ascraeus Montes the ends of the second and first stages, respectively, implying that Arsia is the oldest, and Ascraeus the youngest, of the three Tharsis Montes.

[10] *Bleacher et al.* [2007a] also found that rift apron lavas are superposed upon those of the main shield, suggesting that the majority of their formation likely post-dated the main shield-building phase. Crater counts indicate that this phase occurred during the middle Amazonian, at least $\sim$1 to $\sim$1.5 Ga ago, with the latest units resurfacing the flanks during the late Amazonian [*Plescia and Saunders*, 1979; *Neukum and Hiller*, 1981; *Hiesinger et al.*, 2007]. Together, these results suggest a volcanic and structural sequence of development for Ascraeus Mons that featured (1) a period of main shield building, (2) the construction of rift aprons to the

northeast and southwest, and (3) late-stage resurfacing in the Amazonian.

2.1. Surface Features Studied in This Work

[11] The abundance of well-preserved features on the surface of Ascraeus Mons makes this volcano a suitable case study for understanding the constructional histories of the Tharsis Montes. We examine in detail six types of prominent surface feature: the caldera complex, flank terraces, pit craters, sinuous rilles, arcuate grabens, and small vents.

2.1.1. Caldera Complex

[12] The main Ascraeus shield is largely symmetric about the caldera complex [*Zimbelman and Edgett*, 1992], which is perhaps its most prominent feature (Figure 2a). The calderas are steep-sided, overlapping structures with both terraced and slumped walls (Figure 2a: 1), while the caldera floors are generally flat and featureless [*Crumpler and Aubele*, 1978; *Zimbelman and Edgett*, 1992; *Crumpler et al.* 1996] (Figure 2a: 2).

[13] *Crumpler and Aubele* [1978] reported three calderas based on limited Viking Orbiter data, while *Crumpler et al.* [1996] described at least four. *Mouginis-Mark* [1981] identified eight discrete collapse features sourced from both peripheral and central magma chambers, as did *Zimbelman and McAllister* [1985] and *Scott and Wilson* [2000]. Using Mars Odyssey THEMIS data, however, *Mouginis-Mark and Christensen* [2005] reported that at least eleven collapse events had occurred within the caldera complex. More recently, *Werner* [2009] counted at least six calderas on HRSC images, while *Robbins et al.* [2011] listed seven using CTX data.

[14] Caldera formation is generally accepted to be the result of volume changes in underlying magma chambers, either due to the eruption or lateral migration of material [*Branney*, 1995; *Roche et al.*, 2001; *Walter and Troll*, 2001]. The plan view shape of the caldera often reflects that of the chamber below, though regional stresses may also play a role [e.g., *Crumpler et al.*, 1996; *Holohan et al.*, 2005].

2.1.2. Flank Terraces

[15] Flank terraces are topographically subtle, laterally extensive structures that occur on at least nine large shield volcanoes across Mars [*Byrne et al.*, 2007]. They are outward-verging, convex-upward structures that form a characteristic, imbricate pattern on each volcano they occur.

[16] Terraces were first reported on Ascraeus Mons by *Thomas et al.* [1990] (Figure 2b), who concluded that compression of the volcano due to self-loading led to terrace formation. *McGovern and Solomon* [1993] also found that terraces were compressive structures but related them instead to lithospheric flexure, while *Crumpler et al.* [1996] proposed that magma chamber tumescence was the responsible mechanism. Other workers have argued for an extensional origin for terraces, via gravitational spreading [*Cipa et al.*, 1996] or flank stress relaxation [*Montési*, 2000], whereas *Morgan and McGovern* [2005] and *McGovern and Morgan* [2009] suggested that the terraces on Olympus Mons are due to both thrust faulting and slumping as the edifice spread. In a recent study of MOLA-derived slope maps, *Byrne et al.* [2009] concluded that lithospheric flexure is the most likely terrace formation mechanism, in agreement with *McGovern and Solomon* [1993].

[17] High on the south flank, a mare-like wrinkle ridge circumferential to the summit complex resembles ridges on Pavonis Mons' summit, and may also have formed due to flexure [*McGovern and Solomon*, 1993]. Alternatively, broad summit subsidence or magma chamber tumescence could have been responsible [*Crumpler et al.*, 1996].

2.1.3. Pit Structures

[18] Pit crater chains, while also present on Arsia and Pavonis, are much more prevalent on Ascraeus [*Hodges and Moore*, 1994]. Here, they coalesce into radial or sub-radial grabens that, in turn, form the large, V-shaped vermiform embayments on the southwest and northeast flanks of the volcano [*Zimbelman and Edgett*, 1992]. Circular, near circular, or ovoid depressions, pit craters are distinguished from simple impact craters by the lack of a raised rim around the concavity (Figure 2c). Aligned groups of pits form linear crater chains, and chains can combine to form contiguous trough-like structures [*Crumpler and Aubele*, 1978].

[19] A consensus exists that pit craters are formed by collapse into subsurface voids. Various processes responsible for the origin of these voids have been suggested, including formation due to dyke swarm emplacement [*Mège and Masson*, 1996], karst dissolution [*Spencer and Fanale*, 1990], or by extensional tectonics, either with tensional fracturing [*Tanaka and Golombek*, 1989] or dilational normal faulting [*Wyrick et al.*, 2004].

2.1.4. Sinuous Rilles

[20] Another common surface feature, rilles are rimless, sinuous channels that are usually narrower than pit troughs (Figure 2d). Like the pit craters on Ascraeus, the larger sinuous rilles are mainly concentrated in the embayments, particularly that to the northeast. Smaller sinuous channels also occur within lava flow fields across the volcano [*Mouginis-Mark and Christensen*, 2005]. Both types of structure closely resemble rilles observed on the Moon, both in terms of length and sinuosity [*Mouginis-Mark et al.*, 1984].

[21] Volcanic processes such as ash flow erosion [*Cameron*, 1964], lava tube collapse [*Greeley*, 1971], and lava flow emplacement [*Gornitz*, 1973; *Hulme*, 1973; *Chen et al.*, 2008] have been suggested as potential sinuous rille-forming mechanisms. Conversely, *Peale et al.* [1968] proposed that surface water flow might have led to rille formation, a view shared by *Scott and Wilson* [1999], *Mouginis-Mark and Christensen* [2005], and latterly *Murray et al.* [2010], who suggested that rilles on Ascraeus Mons were formed when groundwater breached the surface of the volcano from fractures within the edifice.

2.1.5. Arcuate Grabens

[22] *Crumpler and Aubele* [1978] observed abundant concentric grabens on the flanks of Arsia and Pavonis Montes, but very few on Ascraeus. They noted, however, that while pit craters occur more frequently on Ascraeus, they share a similar distribution with the grabens on the other Montes. They also reported a series of closely spaced arcuate troughs on the smooth plains to the northeast of Pavonis Mons (Figure 2e), but lacked data for the plains surrounding Ascraeus. Nonetheless, such structures were reported for this volcano by *Scott et al.* [1981] and *Comer et al.* [1985].

[23] Load-centric, arcuate grabens are predicted to form due to extension of the crust along a topographic bulge as a

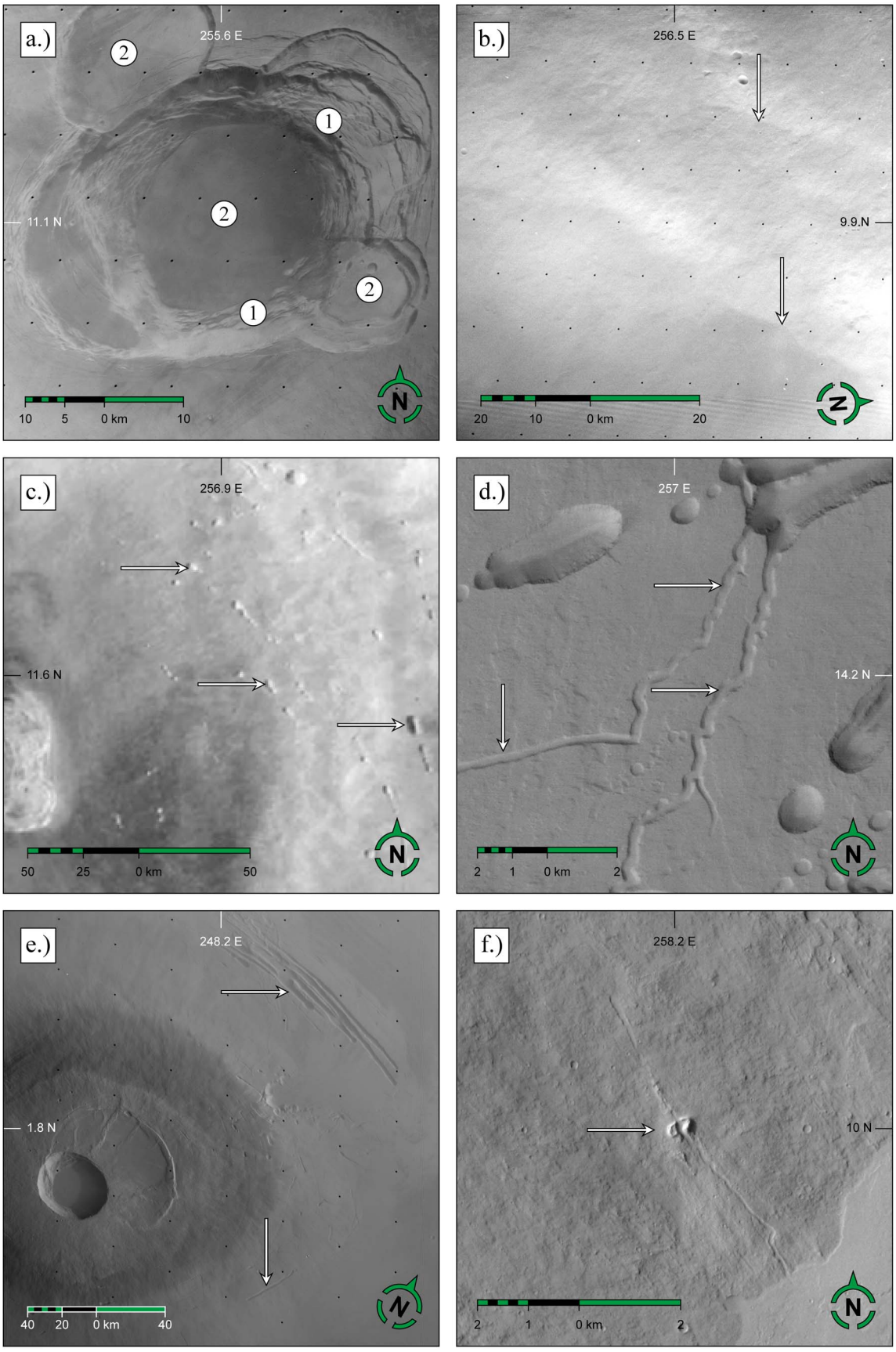
a.)
255.6 E
11.1 N
10 5 0 km 10
b.)
256.5 E
9.9.N
20 10 0 km 20
c.)
256.9 E
11.6 N
50 25 0 km 50
d.)
257 E
14.2 N
2 1 0 km 2
e.)
248.2 E
1.8 N
40 20 0 km 40
f.)
258.2 E
10 N
2 1 0 km 2

Figure 2

Table 1. Details of the Photogeological Images Used in This Study

Image Number	Resolution (m/px)	Coverage
	HRSC	
h0016_0008	12.3	E side of caldera and E proximal flank
h0068_0000	12.4	Caldera and volcano center
h1206_0001	12.2	Medial W flank southwest embayment
h1217_0001	12.1	Distal W flank and plains
h2032_0001	12.2	Distal E flank and plains
h2054_0001	12.2	Medial E flank and NE embayment
	CTX	
P02_001708_1889	5.1	SW embayment
P06_003330_1890	5.1	Medial W flank and SW embayment
P13_006165_1914	5.1	Medial W flank and SW embayment

volcano down-flexes its underlying basement [*Thurber and Toksöz*, 1978; *Schultz and Zuber*, 1994; *Williams and Zuber*, 1995]. Their radial positions with respect to a load can be used to estimate the elastic thickness of the supporting crust [e.g., *Comer et al.*, 1985].

2.1.6. Small Vents

[24] The flanks of Ascraeus Mons have been noted for the paucity of parasitic vents and cones [*Mouginis-Mark*, 1981; *Mouginis-Mark and Christensen*, 2005; *Murray et al.*, 2010], though *Bleacher et al.* [2007a] noted extensive small-vent fields beginning some 120 km from the main shield. (A similar vent field lies to the south of the main Pavonis Mons shield [*Bleacher et al.*, 2009], though Arsia Mons is without such a feature [*Mouginis-Mark*, 2003].) Except where truncated by the caldera complex, the proximal regions of most lava flows on Ascraeus are buried by successive volcanism or merge with hummocky and mottled units, as described by *Bleacher et al.* [2007a].

[25] *Mouginis-Mark and Christensen* [2005] identified a single putative cinder cone on the south flank of Ascraeus astride a linear structure (Figure 2f), while *Murray et al.* [2010] added to this observation by reporting a pair of cones 150 km northeast of the caldera center; each of these features is heavily eroded, however. Such features, commonly observed on Terran volcanoes [e.g., *Clarke et al.*, 2009], would be expected to form even with magma of very low volatile content [*Wilson and Head*, 1994]. Nonetheless, those structures that have been observed may be remnants of an earlier, gas-rich eruptive phase [*Murray et al.*, 2010].

3. Methodology

[26] We used the three-dimensional Mars Global Surveyor MOLA [*Zuber et al.*, 1992; *Smith et al.*, 2001] 128 pixel/degree Digital Terrain Model (DTM) topographic data set as the base map for a GIS. The ESA's Mars Express HRSC [*Neukum et al.*, 2004] provided the primary photogeological data set in this study, as HRSC images offer extensive spatial coverage of the volcano at a nadir resolution of approximately 12 m/pixel. Data from NASA's Mars Reconnaissance Orbiter CTX experiment [*Malin et al.*, 2007], with a resolution of ca. 5 m/px, were used to supplement data loss on HRSC image h1206_0001. Details of the photogeological images used in this study are listed in Table 1.

[27] ESRI ArcCatalog 9.1 was used to apply the IAU 2000 geographic coordinate system for Mars to all photogeological data, which were then assigned an orthographic sinusoidal projection with an east positive center of longitude of 255.0°. The HRSC and CTX images were georeferenced to the MOLA elevation data and rectified in ESRI ArcMap 9.1, producing the photomosaic that is shown in Figure 3.

[28] All surface features, with the exception of flank terraces, were mapped into polyline and polygon vector shapefiles from the HRSC and CTX data, using ArcMap 9.1's Editor and Advanced Editor functions. Shapefiles were grouped by feature into separate mapping layers. Most mapping was performed at a constant view scale of 1:30,000; this mapping scale was chosen as it offered a good compromise between including larger, relevant structures, and incorporating those that are too small to warrant consideration for this study. More expansive features, e.g., the large grabens to the northwest of the volcano, were mapped at a view scale of 1:70,000.

[29] Features below approx. 200 m in diameter were ignored, as were those whose provenance or extent was ambiguous due to low quality imaging, erosion, or inundation

Figure 2. The surface features examined in this study. (a) The Viking Orbiter data used by *Crumpler et al.* [1996] to investigate Ascraeus Mons' summit caldera complex. Illumination is from the northeast (frame 090A50). Extensive terracing and slumping (1) has rendered each caldera structurally complicated, in contrast to the generally smooth and featureless caldera floors (2). (b) A Viking Orbiter image previously used to study the flank terraces on Ascraeus Mons [*Carr et al.*, 1977; *Thomas et al.*, 1990], illuminated from the east (frame 210A15). Visible terrace outlines are marked by white arrows. (c) An example [after *Wyrick et al.*, 2004] of pit crater structures, shown here by arrows, on the upper eastern flank on Ascraeus Mons. The flank slopes to the right of the image (MOC frame FHA01415). Illumination is from the west. The eastern sector of the caldera complex is visible to the left. (d) A set of sinuous rilles on the northeast flank of Ascraeus, described by *Murray et al.* [2010]. (HRSC image h0016_0008, illuminated from the southwest.) The rilles are sinuous channels that change direction abruptly (highlighted here with white arrows), which crosscut flank lavas but are, in turn, truncated by surrounding pit craters. (e) Extensive arcuate grabens occur to the northeast of Pavonis Mons, as well as on its eastern flank (highlighted here with arrows). This Viking Orbiter image shows almost the entire Pavonis volcano, with the prominent caldera complex visible to the lower left. Similar to Ascraeus, Pavonis Mons has embayments on its lower flanks (the northeast embayment is visible near the center of this image, part of frame 643A54). Illumination is from the east. (f) The dissected vent (arrowed) on the southeast flank of Ascraeus described by *Mouginis-Mark and Christensen* [2005] and *Murray et al.* [2010] (THEMIS frame V11250004, illuminated from the west). The cone is bisected by a linear structural feature that Mouginis-Mark and Christensen suggested could be the surface expression of a dike or a small spatter ridge, but which we map as a sinuous rille (see section 4.6).

Figure 3. Photomosaic of the HRSC and CTX images used in this study. The broad, vertical strips are HRSC data, while the diagonal, thinner strips are CTX. Arranged left to right, portions of HRSC images h1217_0001, h1206_0001, h0068_0000, h0016_0008, h2054_0001, and h2032_0001 are used. CTX images P02_001708_1889, P06_003330_1890, and P13_006165_1914 complement HRSC. The map is displayed in a sinusoidal projection, with an east positive center of longitude of 255.0°. The boxes indicate the locations of Figures 5a, 6a, 6b, 7a, 7b, 8a, 8b, 9, 10a, and 10b. The terraces on the southeast flank are particularly prominent in this mosaic (1, see section 4.2).

by later volcanics. Only those with discrete boundaries were mapped as individual features, e.g., pit craters within a larger collapse trough were regarded as belonging to that same trough, and were not counted separately, nor were individual structures within the caldera complex such as fractures, grabens, and pits. Additionally, the scalloped texture on the volcano's northwest flank did not allow unequivocal distinction between pit crater structures and collapse terrain unrelated to tectonic processes. The total number of pit craters presented in this study, therefore, is likely to underrepresent the actual quantity of pits on Ascraeus Mons. In addition, only those narrow, meandering channels within lava flow fields without levees were classified as sinuous rilles.

[30] Because most flank terraces are not readily visible on two-dimensional photogeological images [*Thomas et al.*,

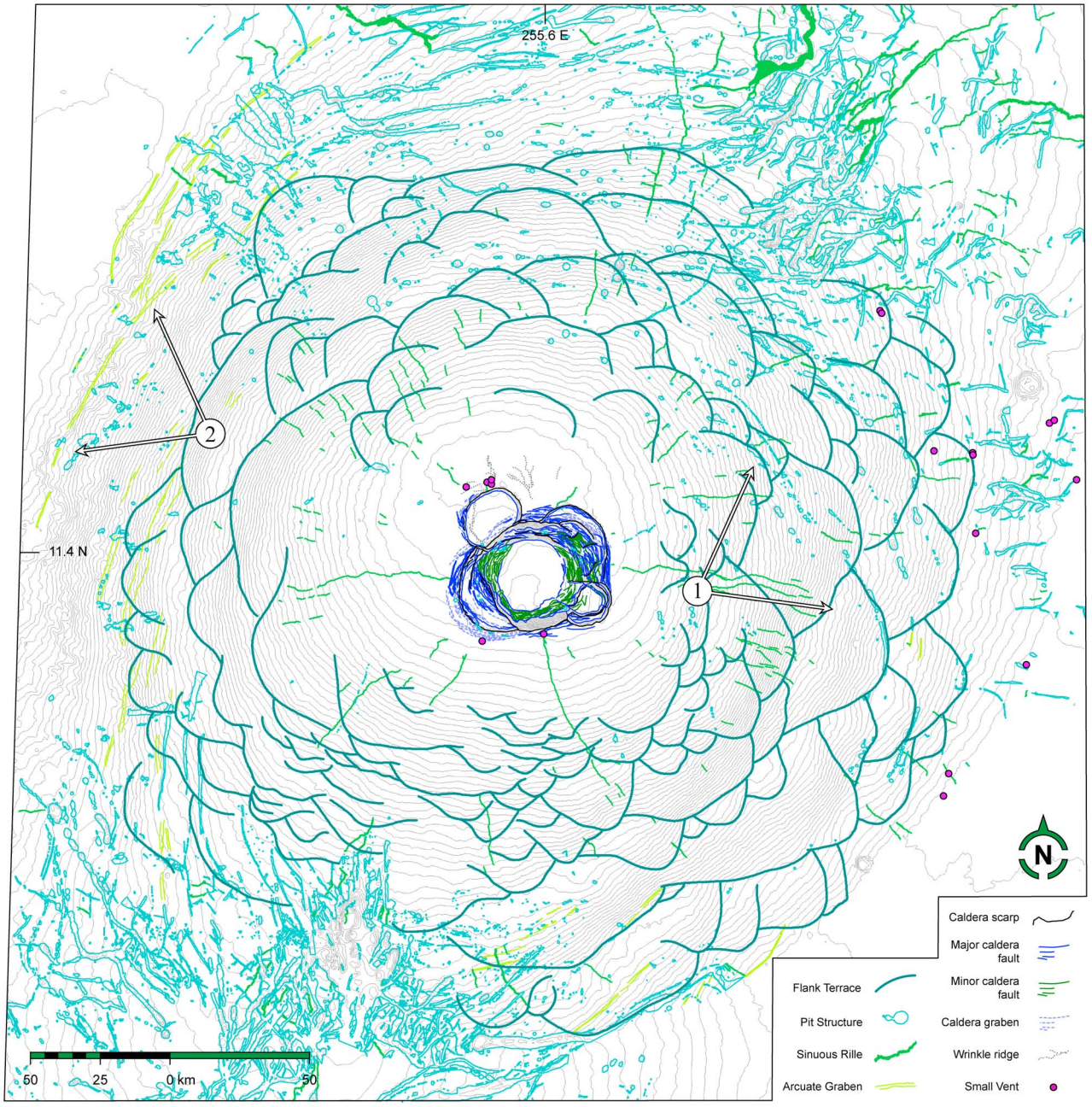

Figure 4. The full set of surface features on Ascraeus mapped in this study. The color scheme shown here for each feature type is used for every successive figure. This composite map has the same projected coordinate system as that in Figure 8. Additionally, this figure is shown with a 250 m contour map of the volcano for spatial context. In places, separate crater chains appear to can form laterally contiguous structures over several tens of kilometers across the volcano (1, see section 4.3). Similar to the pit crater structures, some grabens appear to be aligned, and may be discrete surface expressions of larger structures (2, see section 4.5).

1990], the terrace outlines for Ascraeus were mapped from MOLA-derived slope maps with a cell size of ~460 m, following the methodology of the terrace study by *Byrne et al.* [2009]. The terrace map of Ascraeus Mons was integrated with the other mapping layers in the GIS. In the few instances where terrace boundaries were clearly visible on the photogeological data, the MOLA-based map was modified accordingly.

[31] Finally, the purpose of this survey is not to exhaustively characterize the morphometric and spatial properties of every volcanotectonic element on Ascraeus Mons, but rather to provide a general description of each type of prominent surface feature. Therefore, its results are described in terms sufficient to define the representative shape, size, and location(s) of a given feature set, though quantitative data are provided where appropriate. The ArcGIS shapefiles for each

Table 2. Numbers of Features by Type[a]

Feature Type	Count
Caldera	3 (4)
Flank terrace	144
Pit structure	4,177
Sinuous rille	318
Arcuate graben	161
Small vent	18
Total	4,821 (4,822)

[a]The numbers of discrete features presented here correspond to those that have been unequivocally identified and classified according to feature type. Note, however, that parts of a single structure but apparent as several, e.g., portions of the arcuate grabens encircling Ascraeus Mons, have been counted separately. Additionally, the figure in brackets for the number of calderas on Ascraeus indicates the ambiguity that exists as to whether three or four calderas are present; while three are obvious, we acknowledge the possibility that so too does a fourth.

mapping layer, and associated attribute tables, are available for use in more detailed, feature-specific studies by contacting the corresponding author.

4. Observations

[32] A total of 4,821 separate features were mapped on the flanks and rift aprons of Ascraeus Mons; the full set of feature maps are shown together in Figure 4, while full-format . tif maps for each feature set are provided as auxiliary material (Figures S1–S5).[1] A breakdown of this count by feature is given in Table 2. Where quoted, height/depth values were derived from the MOLA DTM, while horizontal length measurements were calculated from the photogeological data.

4.1. Caldera Complex

[33] The summit caldera complex on Ascraeus Mons is 56 km in east–west diameter, and 55 km north–south. It has been the focus of previous studies [*Mouginis-Mark*, 1981; *Zimbelman and McAllister*, 1985; *Zimbelman and Edgett*, 1992; *Scott and Wilson*, 2000; *Mouginis-Mark and Christensen*, 2005; *Werner*, 2009; *Robbins et al.*, 2011], which suggested between three and eleven summit calderas. We observe three unequivocal calderas here, with a possible fourth structure present within the largest depression (Figure 5 and Table 3).

[34] The main caldera is a faceted, roughly elliptical pit, with a near-circular polygonal floor and steep, inward-dipping walls (Figure 5a: 1). This caldera, which has an eccentricity of approximately 0.88 (major axis: 40 km southeast-northwest, minor axis: 35 km southwest-northeast), is encompassed by a southwest-northeast trending elliptical peripheral fault zone [*Branney*, 1995; *Roche et al.*, 2001; *Walter and Troll*, 2001; *Troll et al.* 2002; *Holohan et al.*, 2005]. This zone of extension is characterized by a multitude of collapse pits and a set of linear grabens and half-grabens that define the caldera's polygonal shape (Figure 5a: 2). Throws on their inward-facing bounding walls appear to increase inward (illustrated by progressively taller scarps, though this cannot be reliably measured with MOLA data).

[35] There is a large terraced zone on the northeast side of the main caldera, which features a dense fracture network and numerous faults (Figure 5a: 3). With a semi-elliptical outline, it is possible that this terrace represents the floor of another, nested caldera (Figure 5b: 1). The peripheral fault zone, however, fully encompasses this depression, and it is much more heavily fractured than the two smaller, older calderas despite all three being located on the edge of the central pit. Additionally, as a southwest-northeast elongate structure, the central caldera's peripheral fault zone displays the same orientation as the regional structural trend across the Tharsis Montes. We cannot therefore conclusively determine whether this feature is a discrete, fourth caldera.

[36] A larger, less fractured terrace exists on the southwest wall (Figure 5a: 4). Three intensely faulted zones that resemble bench-like talus deposits occur on the floor of the polygonal pit. The largest is related to the northeast terraced zone and another to the southeast caldera, while the third is on the western edge of the main pit. Fluting occurs along the upper portions of several caldera walls, particularly on the south wall of the central pit (Figure 5a: 5), where some horizontal strata are visible. The lower caldera walls have a more massive texture, indicative of talus slopes.

[37] Two older calderas are visible: one to the northwest (Figure 5a: 6), and a smaller one on the southeast side (Figure 5a: 7). The northern structure is cut by the central caldera's polygonal pit and its peripheral extensional zone. The southeast caldera is also included within this zone, and has clearly identifiable reverse and vertical faults that are cut by the central pit. A broad concentric terrace runs along its inner wall (Figure 5a: 8).

[38] The caldera floors are generally flat and featureless, though there is a very small rim or ridge near the south edge of the central pit. Another is present in the northwest caldera, where at least one definite wrinkle ridge is also present (Figure 5a: 9). The main caldera is 3.3 km in depth (measured from the volcano's summit), while the northwest and southeast depressions are 390 m and 1,770 m deep, respectively. The putative fourth caldera has a depth of 190 m. All calderas, including the possible fourth, have similar aspect ratios (Table 3).

[39] Many radially orientated lava flows and thin sinuous rilles terminate at caldera edges, demonstrating that they were truncated by these vertical collapse events. Some concentric fractures contain possible eruptive vents (see section 4.6), suggesting that in places magma rose along the peripheral extension zones after caldera formation; this is often seen on Terran volcanoes, e.g., the Galapagos shields and La Réunion.

[40] Several positive topographic structures that resemble wrinkle ridges are present on the planar area to the north of the caldera complex, and trend both radially and concentrically to the volcano (Figure 5a: 10). Many lava flows and tubes can also be recognized, and are readily distinguishable from the ridges.

4.2. Flank Terraces

[41] We counted 144 terraces on the flanks of Ascraeus, which are circumferentially arranged in an imbricate "fish scale" pattern around the volcano but are most prominent on the northwest and the southeast flanks (Figure 3). On these flanks, despite being draped in lava flows, terrace boundaries

[1]Auxiliary materials are available with the HTML. doi:10.1029/2011JE003825.

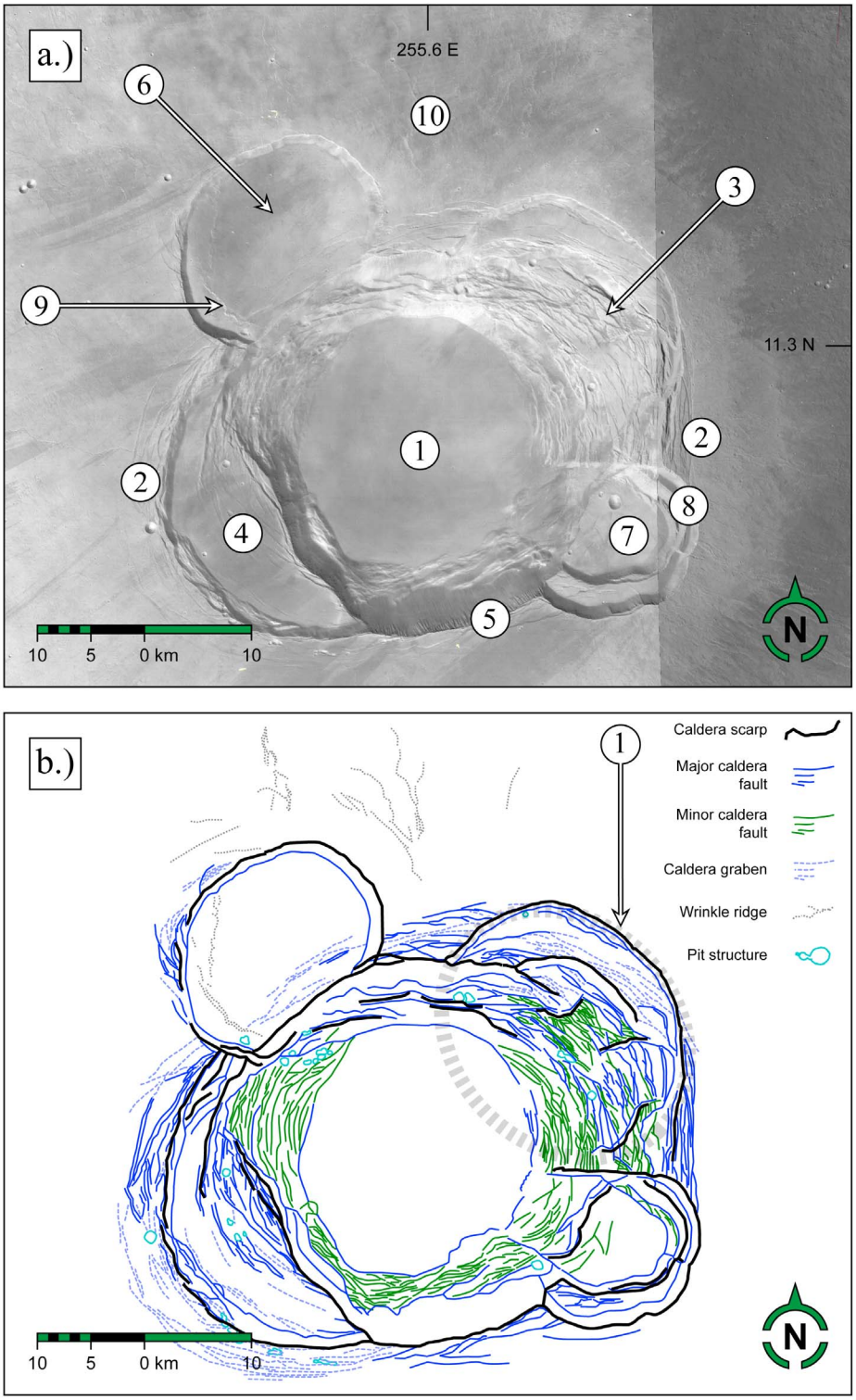

Figure 5. The summit caldera complex on Ascraeus Mons. (a) HRSC mosaic of the summit caldera complex on Ascraeus, illuminated from the southwest (HRSC images h0068_0000 and h0016_0008). Dominating the structure is the central polygonal pit (1), enclosed by an elliptical peripheral fault zone (2). The large, fractured terraces within the main caldera are also clearly visible (3 and 4). Fluting is evident along the upper walls of the main caldera (5). Two truncated calderas lie to the northwest and southeast (6 and 7, respectively). At least two incidences of collapse have occurred within the south-southeast caldera (8). Surface contraction has led to the formation of wrinkle ridges in the northwest caldera (9) and on the adjoining summit plateau (10). (b) The structures of the caldera complex mapped in this study. The dashed ellipse indicates the position of a putative fourth caldera within the summit complex (1).

Table 3. Caldera Morphometry Data

Caldera	Long Axis (km)	Long Axis Orientation	Short Axis (km)	Short Axis Orientation	Aspect Ratio	Depth (m)
1	58	SW-NE	40	NW-SE	1.45	3,300
2	24	SW-NE	17	NW-SE	1.41	390
3	19	SW-NE	14	NW-SE	1.36	1,770
(4)	(29)	(NW-SE)	(20)	(SE-NE)	(1.45)	(190)

remain perceptible (Figure 3: 1), while on others, lavas have obscured terrace morphology and render them visible only on slope maps. Flank terraces are broad, positive-topographic structures typically several tens of kilometers in circumferential length, but often with vertical heights of only several hundred meters (Table 4). Terraces do not appear on either rift apron. In eleven places, there is a spatial correlation between terrace boundaries and pit crater chains and grabens (Figure 6a).

[42] The wrinkle-ridge structure high on the south flank of Ascraeus, first noted by *Crumpler et al.* [1996] and orientated circumferential to the summit (Figure 6b), fits closely with the trace of a terrace identified using MOLA slope data. Its leading edge is an outward-verging, somewhat sinuous arcuate scarp (Figure 6b: 1). The ridge is approximately 55 km in circumferential length, with a radial width of two km. Superposed upon it is a multitude of smaller, sub-parallel wrinkle structures (Figure 6b: 2). A back scarp faces toward the summit (Figure 5b: 3). This is discontinuous and disappears at a radially orientated lava flow, which is itself cut by the outward facing scarp (Figure 6b: 4). The ridge is approximately 180 m taller than the surrounding flanks.

4.3. Pit Structures

[43] A total of 4,177 pit structures were counted on our HRSC-CTX mosaic of Ascraeus Mons, including individual pit craters, pit crater chains, and coalesced trough structures (Figure 4). Pit craters range from circular to elliptical in plan view shape (Figure 7a: 1). As reported by *Crumpler and Aubele* [1978], rows of three or more pits in alignment form crater chains (Figure 7a: 2), and crater chains can, in turn, merge to form troughs (Figure 7a: 3). Some pits are conical-shaped depressions that taper to a point, but most craters and troughs display U-shaped or flat floors.

[44] Stratification is often evident within the walls of pit craters, with fluting and slumping of upper units producing talus slopes and deposits on the crater floors, similar to that observed within the calderas of Ascraeus and Pavonis Montes [*Crumpler and Aubele*, 1978] (see section 4.1). Scarps resembling normal faults often bound crater chains and troughs, resulting in a scalloped appearance. Such faults can also cause terracing along the inner walls of troughs, and may even aid trough development by facilitating the collapse of material along them (Figure 7a: 4). Pit structures are superposed upon surrounding lava units, though in no cases do flows appear to have issued from the pit themselves.

[45] Pit craters, chains, and troughs occur all across the surface of Ascraeus, from the middle flanks onto the rift aprons, but are concentrated on the northeast and southwest sectors. Furthermore, pit crater chains are almost exclusively restricted to the flanks, while troughs are particularly prominent on the rift aprons, mainly to the north and southwest. In contrast, pit chains and craters are not as abundant on the aprons. Pit chain and trough orientations on the upper flanks are largely volcano-concentric, but tend toward radial orientations at lower flank elevations and with increasing proximity to the embayment complexes. Some chains are not completely concentric but are instead tangential and cut across the slope, while several discrete chains are aligned with one another despite being separated by several tens of kilometers, forming a linear set of structures that extend across the volcano (Figure 4: 1). Within the flank embayments, individual troughs may exhibit a range of orientations and abrupt changes in direction, although the overall embayment complexes are radial to the volcano. As noted above, there are also eleven discrete instances where pit chains and troughs follow the breaks in slope where one terrace meets another, hence postdating the flows that mantle the base of the terraces (Figure 6a).

[46] Pit crater dimensions vary widely. Individual pit diameters range from 190 m to 3,050 m, while pit troughs are from 400 m to 55 km in length. The depths of these structures are more consistent, however, varying only between several tens to hundreds of meters. Note that these values are considered representative of the general pit crater population on Ascraeus Mons, as we do not provide morphometric data for every pit structure on the volcano. Moreover, establishing the dimensions of the larger coalesced pit structures is more difficult. For example, we have mapped the Ascraeus Chasmata embayment as a single, vermiform structure with multiple orientations, depths, and widths (Figure 4).

[47] Within Ascraeus Chasmata (the southwestern embayment), we observed a 630 m long southeast-northwest trending graben situated on a promontory bounded by two sub-radial troughs (Figure 7b). Where the troughs meet, their walls provide a three-dimensional cross-section of this part of the volcano (particularly to the southeast where lighting conditions are favorable) and thus a unique insight into the internal stratigraphy of the volcano (an approach similar to that utilized by *Mouginis-Mark and Rowland* [2008] to investigate the constructional history of Arsia Mons). The

Table 4. Mean Values for Flank Terrace Morphometric Properties[a]

Parameter	Value
Number	144
Bounding Length (km)	39.6
Circumferential Length (km)	31.9
Radial Length (km)	9.6
Vertical Height (m)	1,084
Slope (°)	6.2
Elevation (m)	
min:	3,874
max:	17,300
Elevation range (%)	
min:	4
max:	94

[a]The values presented here are after *Byrne et al.* [2009], where the various morphometric parameters of flank terraces are discussed. The terrace number is the total number of unequivocal terrace structures mapped per volcano. Bounding, circumferential, and radial length values are rounded to the nearest hundred meters. Vertical height and elevation minima and maxima values are given to the nearest whole meter. Slope values to the first decimal point are presented. Elevation minima and maxima values are relative to the IAU2000 definition for Mars. Elevation percentage ranges are calculated according to the relief values from *Plescia* [2004].

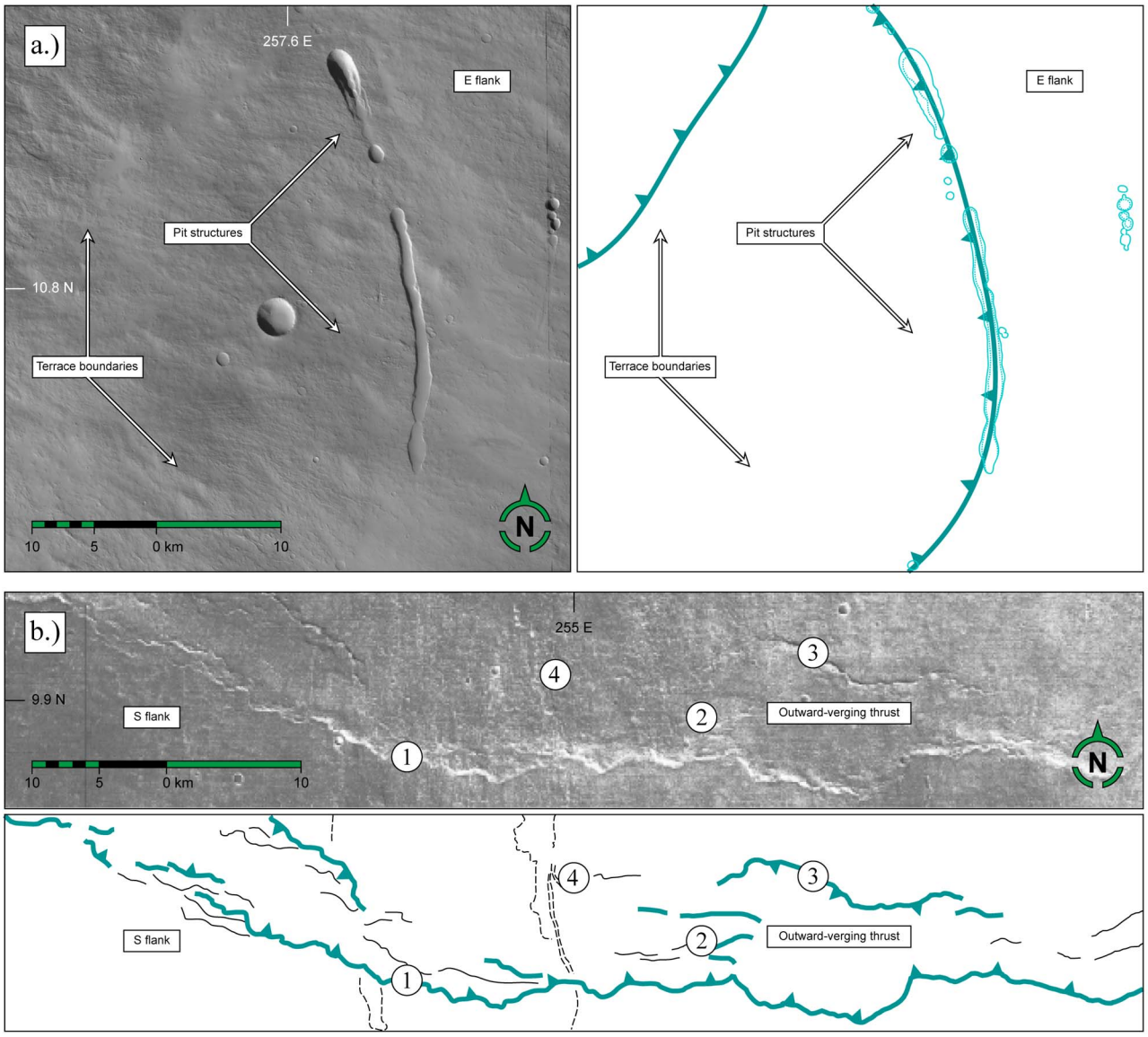

Figure 6. Examples of compressional flank tectonism on Ascraeus Mons, shown by photogeological data accompanied by interpretative sketches. (a) An instance where pit crater structures (solid outlines, with floors delineated by dashed lines) are spatially coincident with flank terrace boundaries (heavier lines, with closed teeth showing the presumed direction of throw). (HRSC image h2054_0001, lit from the southwest.) (b) A portion of HRSC image h0068_0000, illuminated from the south, showing the south flank thrust system, which has an arcuate front scarp (1), sub-parallel wrinkle ridges (2), and back scarp (3) that terminates at a summit-derived tabular lava flow (dashed, 4).

graben's inward-dipping bounding faults are visible (Figure 7b: 1), and measurements derived from the photogeological data indicate that the vertical throw on these normal faults is ca. 10 m. Here, as for the caldera complex, the upper section of the stratigraphy is dominated by a thick packet of lavas within which some individual strata are visible (Figure 7b: 2). Beneath these flows there is a marked change in texture, with the lower, smoother portion of the trough walls again corresponding to talus slopes (Figure 7b: 3). It is at this interface, some 400 m below the surface, that the bounding faults meet (Figure 7b: 4). The south side of the graben is a simple scarp, while the north side has several terraces and a potentially thrusted base. Material has also slumped to the graben floor along the north bounding fault.

4.4. Sinuous Rilles

[48] The majority of the sinuous rilles on Ascraeus Mons are radially oriented, with the greatest concentrations radial to the summit and on the northeast flank (Figure 4). We mapped 318 rilles on Ascraeus, though this count may include segments of longer features obscured by later volcanism, erosion, or aeolian deposition, and so the definitive number may be lower. In addition, our basis for identifying rilles is that of a rimless channel with an undulating morphology, and so we draw no distinction between the rilles

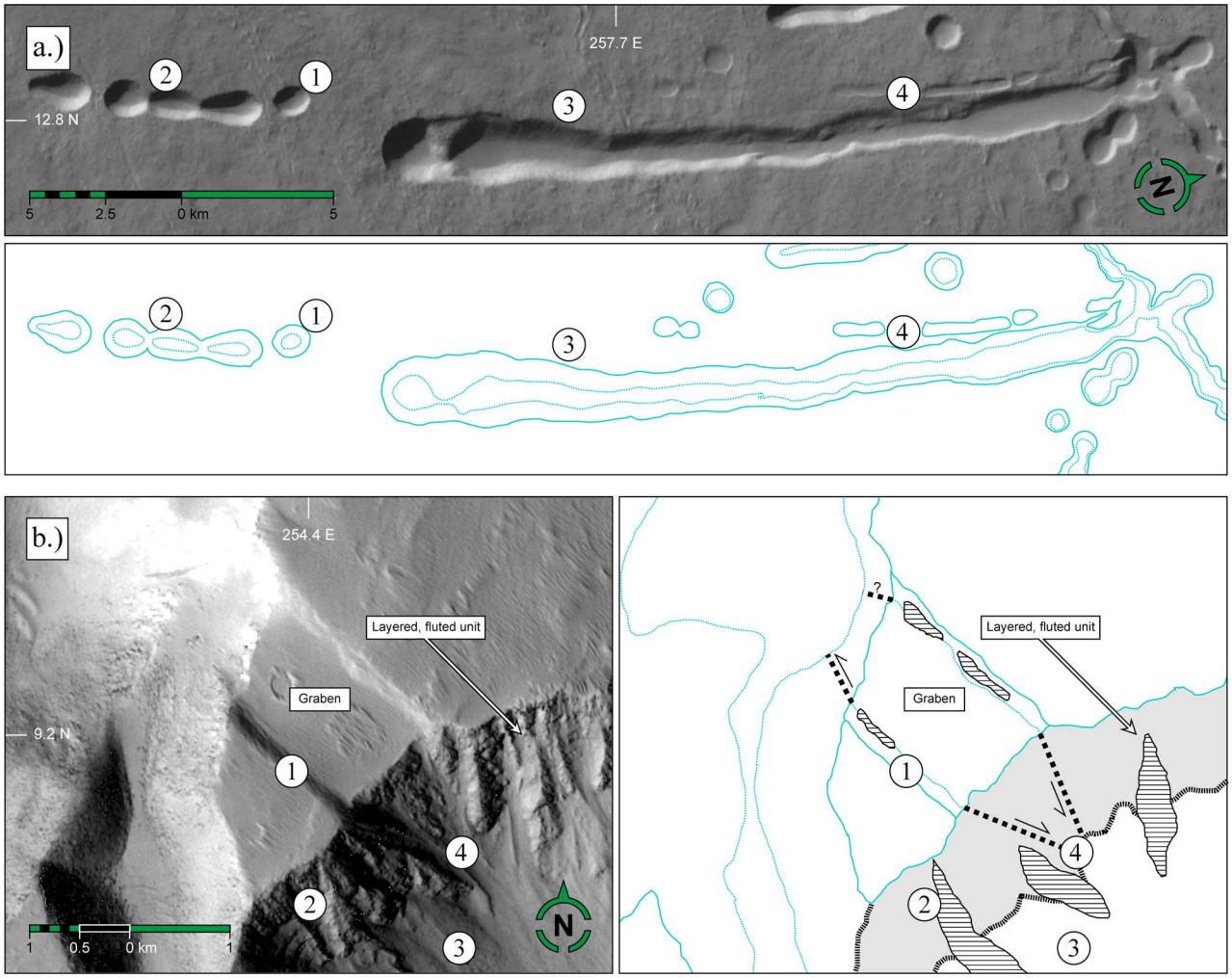

Figure 7. Pit craters on Ascraeus. (a) A group of pit crater structures, including an individual pit crater (1), a crater chain (2), and a coalesced pit crater trough (3). This latter type of structure is commonly bounded by scarps that we interpret as normal faults, and which appear to facilitate trough formation and are often accompanied by talus deposits (4). Portion of HRSC image h2054_0001, illuminated from the northwest. (b) The northwest-southeast trending graben within the southwest Ascraeus Chasmata embayment complex. Erosion has provided a cross-section of this structure (1), which clearly shows a layered, cohesive unit (2) above a more massive unit (3); the graben's bounding faults appear to nucleate at their interface (4). Scree deposits are shown with a horizontal swatch, while the fluted units are illustrated with a gray fill. The structures here are displayed as in Figure 6. CTX image P13_006165_1914, illuminated from the west.

described by *Murray et al.* [2010] and those sinuous channels located within tube-fed lava flow fields on the shield, which are without levees but have been regarded as partially collapsed lava tubes [*Mouginis-Mark and Christensen*, 2005; *Bleacher et al.*, 2007a].

[49] Usually flat-floored structures, rilles, like pit craters, cut across the surrounding lava flows. They can emerge from larger pit crater structures, connect groups of features, and bifurcate from or merge with one other (Figure 8a). Though most rille orientations are radial, some have multiple orientations, abruptly changing from one to another independently of nearby structures or local topography, while their widths and depths remain the same (Figure 8b). In several cases, concentric rilles suddenly alter course and run downslope.

[50] Representative rille dimensions are several hundred meters in width and tens of meters in depth. The largest single rille, however, which occurs within the northeast embayment complex, is 2 km wide and 450 m deep. Rille lengths vary considerably: some of the shorter segments are no more than several hundred meters to a kilometer in length, while the longest example is over 70 km long.

4.5. Arcuate Grabens

[51] On the west and northwest flanks, and extending onto the northwest plains, arcuate grabens extend for ca. 90° concentric to the volcano. Some examples are also present on the southeast flank (Figure 4). They are generally wider, shallower, and more laterally continuous than the coalesced pit troughs observed elsewhere on the volcano, but the

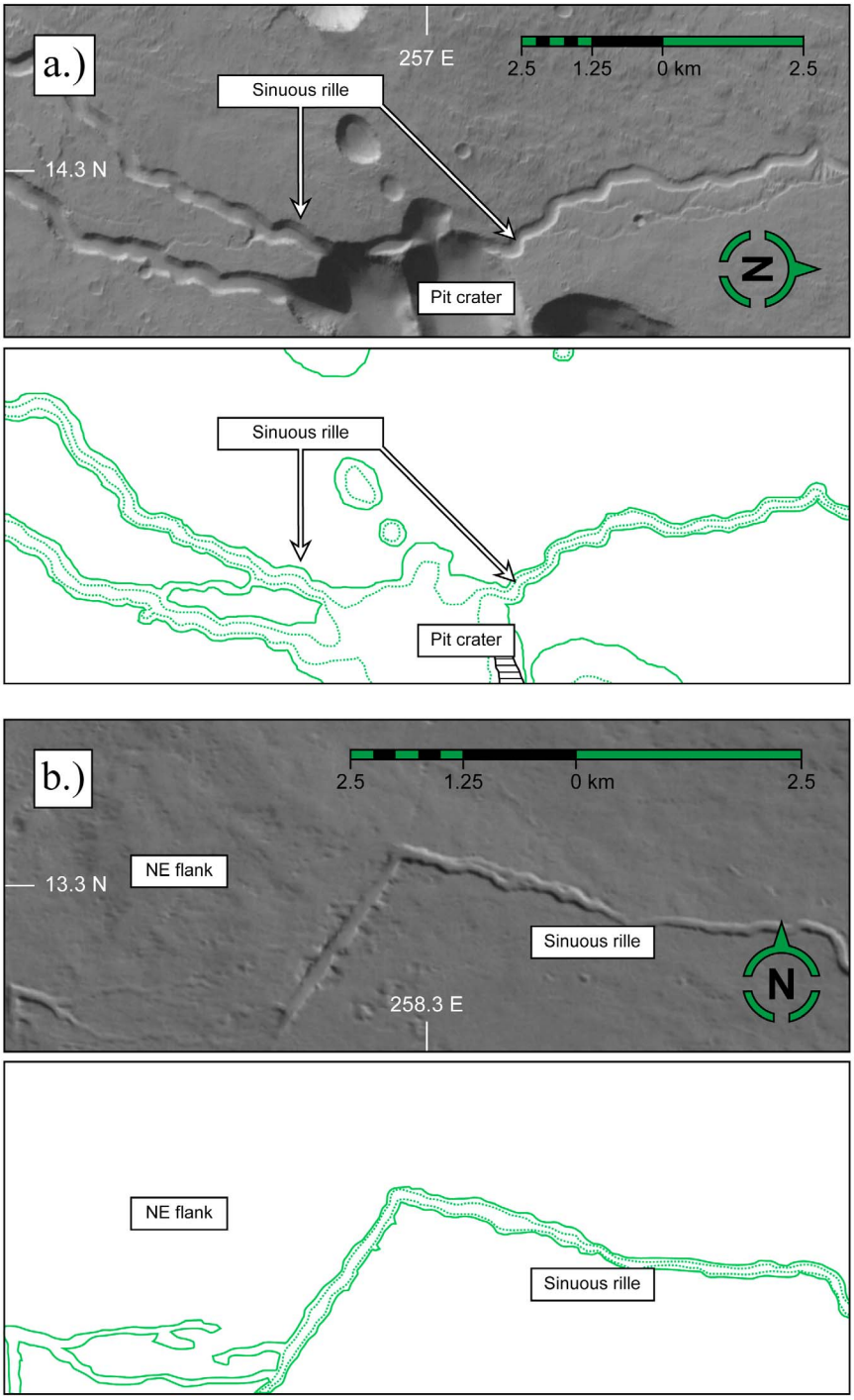

Figure 8. Examples of the sinuous rille on Ascraeus Mons. (a) A sinuous rille on the northeast flank, which intersects the south edge of a pit crater, and reappears beyond the crater's north wall. This portion of HRSC image h2054_0001 is illuminated from the W. (b) Also on the northeast flank, this example displays a prominent and abrupt change in direction, from a bearing of ca. 030° to ca. 120° (HRSC image h2032_0001, illuminated from the south).

cirque-like headwalls and fluted interior walls characteristic of pit crater structures are also absent. They crosscut the plains lavas surrounding the edifice, and in most cases overprint too the collapse material which is possibly sourced from the northwest flank [*Hodges and Moore*, 1994] (Figure 9: 1, 2). We present our mapping results for this feature type in terms of the number of separate, graben-bounding fault traces present on the volcano (Table 2). Therefore, a graben could be said to exist where delineated by two sub-parallel fault traces and where low-angle solar illumination shows the structure to be a negative topographic feature. Yet some aligned but discrete examples may belong

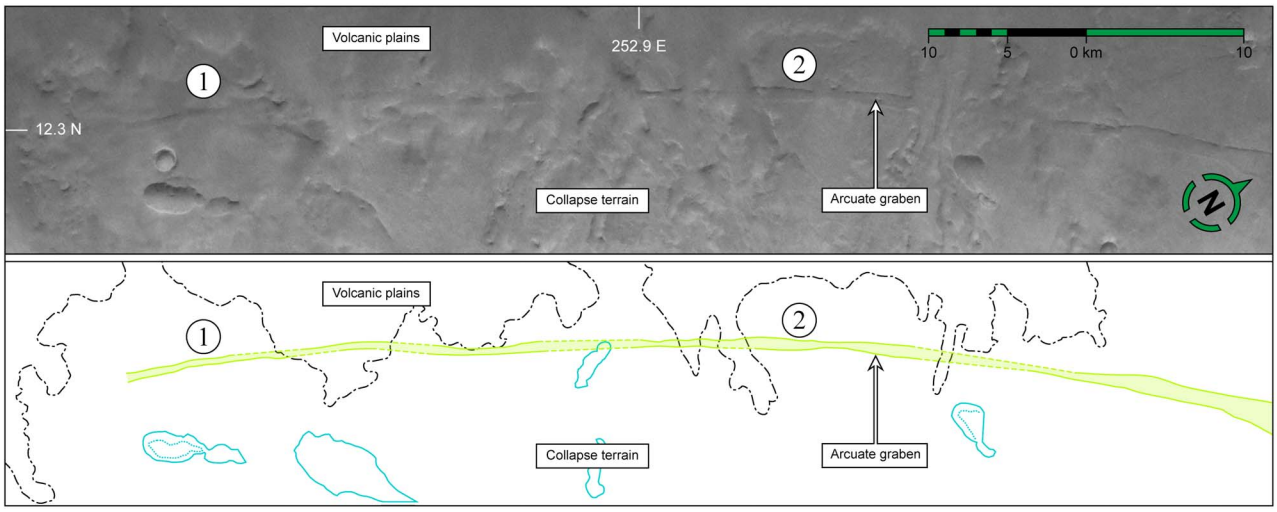

Figure 9. A load-concentric graben to the volcano's northwest, illuminated from the northwest (HRSC image h1217_0001). The graben crosscuts the volcanic plains surrounding Ascraeus Mons, and the collapse material sourced from its northwest flank (1, 2). The area within the graben-bounding fault traces is shaded on the interpretive sketch for ease of viewing.

to a single structure whose surface trace is not contiguous (e.g., Figure 4: 2), and so the total number of arcuate grabens on Ascraeus is unclear. The widths of those structures that are clearly grabens range from 400 m to 1,200 m. Depth values are on the order of 10s to 100s of meters, but in many places, the vertical accuracy of the MOLA data set is not sufficient to resolve these values accurately.

4.6. Small Vents

[52] We observed eighteen discrete vents on the surface of Ascraeus: seven on the summit proximal to the caldera complex, and eleven scattered across the northeast and east flanks (Figure 4) (Table 5). The structures on the summit are largely linear and resemble fissures, and are probably related to nearby lava flows, though several are circular in plan view and may be rootless cones (Figure 10a). Without exception, these appear to have a raised rim. Those on the flanks morphologically correspond to scoria cones (Figure 10b), though some appear largely intact while others have been degraded and tempered by later volcanism. Most vents show no association with any tectonic features. Nonetheless, several are located close to flank terrace boundaries, and at least one straddles a sinuous rille (Figure 10b: 1). The abundance of small vents on the eastern half of the volcano may be an observational bias, as extensive erosion hampers a full assessment of the western flanks.

5. Discussion

5.1. Features

5.1.1. Caldera Complex

[53] We interpret the structure of the summit complex as the product of one major collapse event that followed probably two, but possibly three, smaller, earlier collapses, based on detailed mapping of the caldera structures, experience of calderas on Earth, analog modeling [e.g., *Rymer et al.*, 1998; *Roche et al.*, 2001; *Walter and Troll*, 2001; *Troll et al.*, 2002; *Holohan et al.*, 2005], and comparative studies such as *Branney* [1995]. This view is consistent with those of *Crumpler and Aubele* [1978] and *Crumpler et al.* [1996], but is in contrast to later workers. We suggest that the additional calderas reported by other authors are terraces within, or arcuate slumps formed by sequential collapses of, a larger caldera [cf. *Walter and Troll*, 2001]. Determining the number of discrete collapse events on Ascraeus is of significance in understanding its developmental history. Given an episodic supply of magma and long periods of repose [*Wilson et al.*, 2001], the volcano would require a significantly shorter shield building phase to produce three (or four) calderas than that needed for eleven [*Mouginis-Mark and Christensen*, 2005].

Table 5. Small Vents Morphometry Data[a]

Number	Dimension (m) E-W	Dimension (m) N-S	Type	Flank Elevation (m)	Coordinates Latitude	Coordinates Longitude
2	180	110	Cone (?)	18,180	11.74	255.32
3	220	150	Cone (?)	18,170	11.74	255.33
4	670	570	Fissure	18,150	11.75	255.34
5	170	150	Cone (?)	18,140	11.74	255.34
1	280	1,370	Fissure	18,100	11.72	255.19
6	320	430	Fissure	17,470	10.82	255.67
7	800	230	Fissure	17,300	10.78	255.29
8	410	490	Cone	7,570	12.78	257.78
9	710	560	Cone	7,550	12.79	257.78
10	320	400	Cone	6,810	11.94	258.1
11	330	420	Cone	5,740	11.92	258.35
12	270	180	Cone	5,720	11.91	258.35
13	1,060	540	Cone	5,290	11.44	258.36
14	2,370	1,680	Cone	4,290	12.11	258.82
15	590	530	Cone	3,770	9.97	258.18
17	490	290	Cone	3,700	11.76	258.99
18	230	270	Cone	3,570	9.83	258.15
16	1,440	270	Fissure	3,530	10.63	258.66

[a]Latitude and longitude values are given here relative to a coordinate system with an east positive center of longitude.

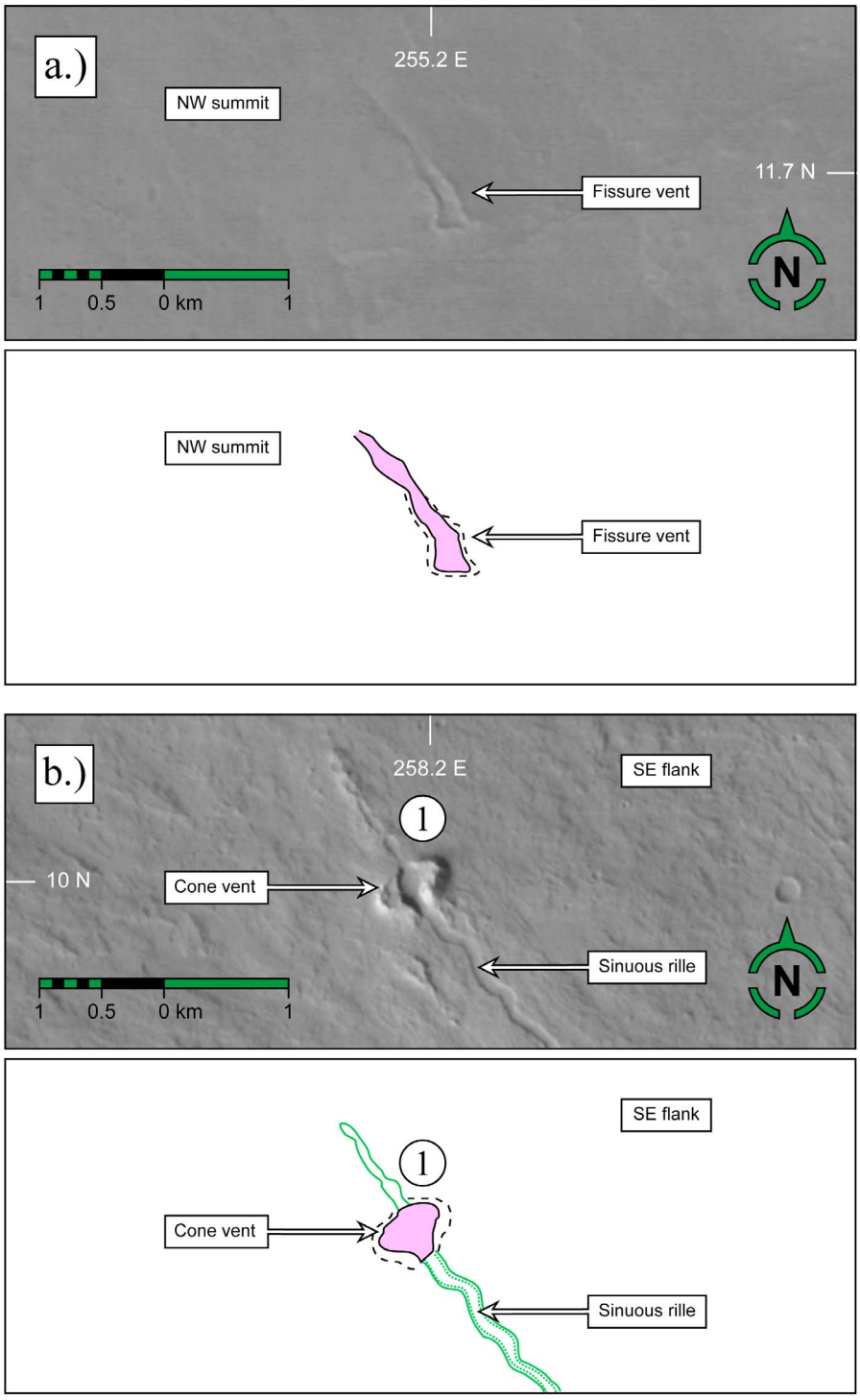

Figure 10. Small vents on Ascraeus Mons, both illuminated from the west. (a) An example of a fissure-like vent located on the summit, to the immediate northwest of the caldera complex. Though largely manifested as a linear depression, there is evidence of a constructional levee to the south of the feature. The figure is a portion of HRSC image h0068_0000. (b) A parasitic vent on Ascraeus, in this case on the southeast flank (the same vent shown in Figure 7, on HRSC swath h2032_0001). This cone has been dissected by a northwest-southeast trending sinuous rille (1).

[54] As most of the area around the caldera consists of flows cut by the peripheral fault zone, and only a few vents are clearly visible, there has been little eruption of material onto the flanks from the summit after caldera formation (although as each caldera may have erupted several times, we refer here to the last instance of activity in each structure). Either eruptive volumes were merely sufficient to resurface the caldera floors only, or the last incidences of collapse were not accompanied by any eruptions at all (e.g., due to sub-surface magma withdrawal [*Mouginis-Mark*, 1981]). The rims and wrinkle ridges in the caldera floors could have been caused by continued subsidence after the initial surface was formed, similar to that reported for the floors of Olympus Mons' calderas by *Zuber and Mouginis-Mark* [1992], and corresponding to the reverse faults observed by *Roche et al.* [2001].

[55] The central polygonal pit is joined to the southwest terrace and northeast fracture zone by a counter-clockwise spiraling geometry, often seen in caldera analog models [*Roche et al.*, 2001; *Holohan et al.*, 2008]. This geometry, together with the peripheral extensional zone, suggests that the entire ensemble is related to one collapse source, and that there is an elliptical, southwest-northeast trending intrusive complex underneath the volcano that has undergone extensive drainage. Terracing and significant extension has occurred to the southwest and northeast, on the long axis of the collapse structure, in contrast to the caldera's steep short-axis sides. Interestingly, that each caldera has a similar plan view aspect ratio (between 1.36 and 1.45, with a mean of $\sim$1.42) suggests that the factors controlling magma chamber geometry were consistent throughout the caldera-forming phase of the volcano.

[56] *Neukum et al.* [2004], *Werner* [2009], and *Robbins et al.* [2011] provide crater ages for the three unequivocal calderas on Ascraeus Mons that are consistent with the caldera formation sequence proposed here, though only the first and third studies enable a comparison with our findings, as they label the calderas for which they present dates. Both these works report that the northwest and southeast structures (Figure 5a: 6, 7, respectively) are older than the central pit (Figure 5a: 1). Both also document a discrepancy between the ages of the terraces within the central caldera (previously regarded as separate calderas) and the central caldera's floor, which we regard as being due to the manner in which the caldera developed. The caldera terraces and faceted pit may have formed during the same collapse event. If this collapse was rapid, they should have similar cratering ages. It is likely, however, that the huge collapse occurred slowly, in which case a central sagging occurred first, with the central block then becoming a progressively more isolated subsidence feature. The terraces would continue to develop via slumping [e.g., *Roche et al.*, 2001; *Geshi et al.*, 2002; *Carter et al.*, 2007]. However, subsequent infilling by lava [*Bleacher et al.*, 2007a], dust, or water could affect these surfaces' derived ages, obscuring any useful relative or absolute age data for the collapse chronology. It is also likely that the largest caldera floor, the smoothest of any on the volcano, was mantled by material that later slumped off the caldera walls. This mantling may have occurred, though to a lesser extent, on the other caldera floors as well.

[57] Evidence for slumping of material onto the caldera floors is provided by the fluted textures and talus slopes visible on the surrounding walls, and the bench-like deposits that lie at their base. The walls themselves provide a three km cross-section of the main shield, similar to the graben within Ascraeus Chasmata but on a larger scale. They show that the transition from layered lavas to talus occurs at varying depths beneath the summit, possibly indicative of a rheological heterogeneity within the volcano. Fractures, hydrothermal alteration, or the inclusion of low-cohesion tephra deposits, unwelded ash, and ice could lead to a progressive decrease in competency with depth [e.g., *Cecchi et al.*, 2004; *Oehler et al.*, 2005; *Donoghue et al.*, 2008]. The abundance of grabens about the caldera complex, and the extent of the fractured slump deposits within, may therefore attest to a volcanic sequence that consists of poorly consolidated and possibly ductile layers (from where the talus slopes begin) underlying a brittle "carapace" of more competent strata (those that display layered lavas). This change in competency may also be applicable to other areas of the volcano where fluted upper units are observed atop talus slopes, e.g., the walls of pit craters and grabens (see section 5.1.3), and could even extend throughout the entire edifice.

5.1.2. Flank Terraces

[58] Despite the range of hypothesized terrace formation mechanisms [*Thomas et al.*, 1990; *McGovern and Solomon*, 1993; *Cipa et al.*, 1996; *Crumpler et al.*, 1996; *Montési*, 2000; *Morgan and McGovern*, 2005], each process can be classified as either compressional or extensional in nature. Based on the convex-upward morphology of terraces, *Byrne et al.* [2009] discounted an extensional origin for these structures [cf. *Cipa et al.*, 1996; *Montési*, 2000]. Of the proposed compressional processes, they did not regard volcano self-loading [*Thomas et al.*, 1990] or magma chamber tumescence [*Crumpler et al.*, 1996] as likely terrace formation candidates. Loading that is restricted solely to an edifice, as envisioned by Thomas and coworkers, will result in an edifice shape evolving from conical to increasingly dome-like. This would be associated with the formation of radially oriented extensional structures, which are not a commonly recognized feature of large Martian shields [e.g., *Crumpler and Aubele*, 1978; *Hodges and Moore*, 1994; *Plescia*, 2004]. Crumpler and co-authors cited simple physical experiments, which showed that magma chamber growth results in the formation of a dome above the chamber [*Marti et al.*, 1994]. The plan view axial symmetry of such a dome, however, does not agree with the distinctive, "fish scale" terrace pattern [*Byrne et al.*, 2009].

[59] These authors in turn favored lithospheric flexure as the formation mechanism for terraces on Martian shields. During flexure, a volcano enters a state of stress where σ_1 is radial, σ_2 is concentric, and σ_3 is vertical [*van Wyk de Vries and Matela*, 1998]. The induced strain results in a net reduction of surface area, accommodated by outward-verging circumferential thrusts [*McGovern and Solomon*, 1993]. We consider these structures to correspond to flank terraces (Figure 4).

[60] Interestingly, the circumferential wrinkle-ridge on the upper south flank of Ascraeus has the same morphological signature as flank terraces on MOLA-derived slope maps of the volcano, and has been mapped as such [*Byrne et al.*, 2009]. Its appearance on HRSC data, including its outward-verging, convex-upward morphology, shows a resemblance

to thrusts seen on volcanoes on Earth [*van Wyk de Vries and Borgia*, 1996; *Borgia and van Wyk de Vries*, 2003; *Mathieu and van Wyk de Vries*, 2009]. Understanding its structure through the synthesis of both data sets gives a useful insight into how the fault, and therefore flank terraces in general, may have formed.

[61] The paired outward- and backward-facing scarps indicate an antithetic fault arrangement relating to a ramp-flat structure [e.g., *Borgia and van Wyk de Vries*, 2003]. Using a fault dip of ∼35° (an approximate value for the angle of internal friction of basaltic lithologies), together with the radial width of the structure, the depth to the detachment surface for this fault anticline is ca. 750 m. The prevalence of wrinkle ridges on the structure indicates that numerous small thrusts were formed as a result of a many- and thinly layered sequence (though the number of thrusts present may be greater than that observed owing to the resolution of the data), and that the entire assembly is the product of upper flank shortening. If so, the whole flank underwent homogenous shortening at first on numerous small, possibly conjugate thrusts. Then, with continued contraction, a major antithetic set increasingly dominated, possibly above a major décollement located almost a kilometer below the surface. This depth is somewhat greater than that of the southwest graben described in 4.3. The many smaller wrinkle ridges on the thrust indicate that there is a multitude of thin alternating competent and incompetent layers within the thrust. Such a situation has been reported at the Paleocene Mull volcano in Scotland [*Mathieu and van Wyk de Vries*, 2009].

[62] The flank terraces on Ascraeus and other volcanoes, therefore, may also have had a thrust morphology, but were mantled and their forms softened by lavas erupted after the onset of flexure. Like the wrinkle-ridge, each terrace might consist of a series of structures instead of one larger fault, though traces of these smaller thrusts may no longer be visible. If the terraces on Ascraeus accommodated a constrictional surface strain upon the volcano, so too did the thrust high on the south flank. As this particular thrust has not been obscured by later lavas, it probably developed after most summit volcanism had ended [*Crumpler and Aubele*, 1978; *Bleacher et al.*, 2007a]. This suggests that flank compression, and thus flexure, continued beyond the end of the main shield-building phase. Moreover, the very small vertical amplitudes of terraces on Ascraeus implies that upper flank shortening may only have been on the order of several percent [*Byrne et al.*, 2009].

[63] The distribution of flank terraces on Ascraeus, specifically the lack of terraces on the northeast and southwest aprons, provides information as to the possible timing of rift apron construction relative to that of the main shield. Terraces can form on shallow gradients such as the flanks of Alba Patera, which have an average flank slope of 1.2°, yet the similarly inclined Ascraeus Mons aprons, with slopes of 1–1.5°, do not display terraces (both slope values are from *Plescia* [2004]). While late-stage resurfacing of the aprons may have obscured what terraces had formed, leaving no trace of them on MOLA slope data, it is also possible that the rift aprons may not have had time to flex the supporting crust and develop flank terraces. If so, this would imply that they are younger than the terraced main shield, a conclusion separately reached by *Crumpler and Aubele* [1978], *Bleacher et al.* [2007a], and *Murray et al.* [2010] based on consistent superposition of main flank lava flows by those sourced from the rift aprons.

5.1.3. Pit Structures

[64] The range of pit structures observed on the flanks of Ascraeus Mons represents a continuum from single, isolated craters to laterally contiguous troughs. In no instance did lavas appear to originate from pits, suggesting that pit crater formation is not related to dyke emplacement [cf. *Mège and Masson*, 1996; *Scott et al.*, 2000; *Liu and Wilson*, 1998]. This finding is consistent with *Wyrick et al.* [2004] in their comprehensive and much larger pit crater-mapping study. Wyrick and co-authors also discounted karst dissolution as responsible for pit formation [*Spencer and Fanale*, 1990] due to a lack of spectroscopic evidence for carbonates co-located with pit craters, and suggested that tensional fracturing [*Tanaka and Golombek*, 1989] may not account for large vertical offsets within pits. They concluded that tensile or hybrid failure along normal faults may produce dilational segments that result in void formation and pit collapse, also suggesting that changes in lithology, dip, and displacement account for the variation in shape and type of structure along strike.

[65] Assuming, then, a dilational faulting origin within a heterolithic stratigraphy, pit craters are proxies for zones of extension within the edifice. Tensional stresses appear to be prevalent across the main flanks and the rift aprons, extending onto the surrounding plains (Figure 4). Prominent flank extension contrasts with the compressional origin of the flank terraces across Ascraeus. In all cases, however, pits are superposed upon terraces, indicating a general change in dominant flank tectonism from compression to extension at some point in the volcano's history (perhaps even prior to the emplacement of the rift aprons). The occasional alignment of pit craters with terrace boundaries (e.g., Figure 6a) implies that pit crater formation occurred due to dilation along fractures previously active as thrust faults within Ascraeus. (As noted in section 3, there may be more pits on Ascraeus than we report here. Nonetheless, we do not expect the true figure to be significantly greater, nor would we expect the difference to have any meaningful effect upon our interpretation of these structures.)

[66] While pit structures may originate due to extensional stresses, other processes have probably acted subsequent to pit formation. Individual pits may represent a single incidence of collapse in which overlying material drains or subsides into a void, with troughs representing aggregates of such collapse events. Within isolated pits and troughs, such as those located high on the flanks, the slumped or collapsed material is constrained by the structure and remains at its base, with further deposition limited to aeolian activity. Yet troughs and pits that occur close to one another may be enlarged by mechanical processes such as sapping [*Laity and Malin*, 1985; *Harrison and Grimm*, 2005; *Irwin et al.*, 2006], by groundwater activity within the volcano [*Murray et al.*, 2010], or by post-formation collapse [e.g., *Bleacher et al.*, 2007a, Figure 4]. These structures could then have coalesced to form contiguous channels through which material can be transported and deposited downslope. We thus envisage individual troughs advancing toward the summit through headward erosion and undermining, while the large embayment complexes to the northeast and

southwest widened with increasing radial distance through trough coalescence.

[67] Textures similar to those seen within the caldera walls are also visible inside many pit craters and troughs across the volcano, i.e., packets of layered, fluted lavas atop massive, smoother talus slopes (e.g., Figure 5a: 5 and Figure 7b: 2), reinforcing the prospect that those flows close to the surface give way to less cohesive/competent units below. This rheological change could in fact exert control over the development of some surface structures akin to thin-skinned tectonics, including the wrinkle-ridge thrust high on the south flank and the small graben within the southwest embayment. Specifically, conjugate faults can nucleate at the interface between two units of differing competencies, and the point at which the southwest graben's bounding faults meet may be at such an interface (in this case at a depth of 400 m). The three-dimensional view accorded by this graben indicates that the fault angles are inclined at about 53°, with a resultant angle of internal friction of approximately 37°. The northwest-southeast orientation of the graben implies slope-parallel radial extension, possibly related to that responsible for pit crater formation elsewhere on the flanks, although its inward-dipping fault planes are strong evidence of a shear component, and not purely dilational faulting.

5.1.4. Sinuous Rilles

[68] In all instances, sinuous rilles crosscut and thus post-date flank and rift apron lavas. In several places, however, rilles have clearly been cut by pit crater structures (Figure 8a), suggesting that while both pits and rilles formed after the lavas, sinuous rilles themselves pre-date the pit craters. Additionally, the latest incidences of caldera subsidence occurred after the formation of those rilles located close to, and originating in, the summit region.

[69] Previous work concluded that sinuous rilles on the Moon are the result of thermal erosion of terrain by high effusion-rate lava flows [*Hulme*, 1973; *Mouginis-Mark et al.*, 1984], and given the morphological similarity between lunar and Martian rilles, similar processes could act on Mars. However, *Murray et al.* [2010] used a flow model adapted from *Williams et al.* [1998] and *Williams et al.* [2005] to calculate the volume of eruptive material necessary to erode a specific rille on the northeast flank of Ascraeus. They determined that at least 5.1 km^3 of lava would have been required to form the channel, and, in the absence of any large flows close to the rille, concluded that lava was not the erosive fluid responsible. They favored water instead, and suggested that a global hydrological cycle could operate on Mars during climatically favorable periods. Murray and coworkers regarded sinuous rilles as channels eroded by groundwater migrating upward through Ascraeus Mons from an ice-rich crust that was heated by magmatic activity within the volcano. This erosion would deposit material downslope, potentially as mudflows and lahars and evinced by braided and meandering channels on the southwest apron, which, in turn, could form the low-angle rift aprons [*Murray et al.*, 2010].

[70] Interestingly, *Bleacher et al.* [2010] examined a > 270 km-long sinuous channel on this same apron that had been previously reported as fluvial [*Mouginis-Mark and Christensen*, 2005; *Bleacher et al.*, 2007a], and found that while the nature of its proximal and medial sections was in fact unclear, its distal section was unequivocally volcanic, and so they concluded that it could have been formed by volcanism alone. Moreover, there is no morphological difference between the smallest rilles that occur within lava flow fields, which appear to have a clear volcanological origin, and the largest examples that populate the flank embayments. This suggests that one process is responsible for the formation of all rilles. If some rilles are formed by fluvial activity, and others are formed by volcanism, it may not be possible to distinguish between the two processes with the data currently available.

[71] Whatever the fluid agent involved, rille orientation and location seem to have been affected in places by surface topography and subsurface structures. The sudden change in direction of some rilles indicates an element of tectonic control, e.g., fluid flowed first along concentric lineaments within the volcano, and then downslope along its surface. Nonetheless, that the majority of rilles are aligned downslope suggests that the extent of tectonic influence upon their orientation is limited and secondary to gravity.

5.1.5. Arcuate Grabens

[72] Concentric to the volcanic load, the long, arcuate grabens to the northwest of Ascraeus cut, and thus post-date, the surrounding lava plains and most aureole deposits at the base of the volcano (Figure 9: 1, 2). The places where grabens do not appear to be laterally contiguous across aureole material may point to a complex history of deposition, or a change in rheology affecting how brittle deformation that leads to graben formation is manifest. The morphological dissimilarity between these structures and the pit troughs elsewhere on the volcano (i.e., the shallow, flat-floored, and contiguous form of the grabens contrasts with that of the deeper, scalloped, and punctuated troughs) suggests that they do not share the same formation mechanism. An extensional origin is likely, however, as they are negative-topographic features and appear to be fault-bounded.

[73] The grabens may correspond to extensional structures predicted to form concentric to a load that flexes its underlying crust, when σ_3 is horizontal and radial [*Comer et al.*, 1985; *McGovern and Solomon*, 1993; *Schultz and Zuber*, 1994; *Williams and Zuber*, 1995; *van Wyk de Vries and Matela*, 1998]. Similar grabens upon the northwest and southeast flanks, and thus within the current radius of Ascraeus, may be remnants of an earlier set of flexural-induced structures, covered by the subsequent growth of the volcano [*Comer et al.*, 1985]. In this case, flexure was an early onset process that continued until at least the end of the main shield-building phase. If the plains material to the northwest of the volcano was emplaced by flows sourced from the rift aprons, then flexure may have continued until at least the start of apron construction. *Comer et al.* [1985] assumed that the grabens on the plains around Ascraeus were caused by flexure, and estimated an elastic lithosphere thickness of between 8 and 50 km, with a best fit of 22 km, based on these structures' radial distances to the volcano.

5.1.6. Small Vents

[74] There are more small vents on the main flanks of Ascraeus Mons than had been previously reported, with potentially yet more on the west flank. Nonetheless, they are not common features, which implies that either degassing occurred before eruption, or that the vast majority of lava flows visible on Ascraeus were emplaced without significant pyroclastic activity (i.e., low volatile content), despite the

consistencies between lava volumes and rheologies with Terran basaltic and andesitic lavas [*Bleacher et al.*, 2007a; *Hiesinger et al.*, 2007]. The lack of vents may also relate to the former compressive nature of the flanks as indicated by the terraces; such a stress state would favor lateral sill formation rather than vertical dykes.

[75] The vents at the summit are almost exclusively fissures (Figure 10a), while those on the flanks are mainly constructional features (Figure 11b). This may indicate a difference in composition between summit- and flank-erupted flows, and could correlate with the contrast in style between eruptions on the main shield and on the flanks reported by *Bleacher et al.* [2007a, 2007b]. Alternatively, erosion by later flows might have degraded summit cones to the point where they are no longer visible. The flank vents may also represent small, parasitic cones formed by the surface eruption of isolated bodies of magma ascending through the volcano as the main phase of shield building ended [*Wolfe et al.*, 1997; *Rowland and Garbeil*, 2000; *Bleacher et al.*, 2007a; *Bleacher and Greeley*, 2008]. The rarity of these features, however, means that determining the precise role they have played in Ascraeus Mons' development remains difficult.

5.2. Geological History

[76] The development of a geological history for any planetary surface is dependent upon clear superposition relationships between surface units and structural features, so that they can be placed within a stratigraphic sequence. On Ascraeus Mons, these relationships exist only for some of the feature types, and so any derived evolutionary sequence is necessarily uncertain.

[77] For example, its distance to other features means it is not clear when the caldera complex formed, or how much time this formation took. Its peripheral fault zone truncates some of the uppermost flow units and sinuous rilles on the volcano, and so the complex's development may partly or even entirely post-date these late features. Another challenge lies in establishing the timing of flank terrace formation. The terraces that remain visible today might represent a single, late-stage increment of shortening upon the volcano's upper surface, or they may be reactivated structures that formed throughout the development of the main shield. Yet another question concerns determining the time at which the arcuate grabens surrounding the volcano formed relative to the sinuous rilles and pit craters on its flanks, as neither of the latter features is crosscut by the former. Moreover, the pits and rilles observed today may be merely the latest populations of these features to form.

[78] We have attempted to resolve some of these uncertainties here. Our knowledge of caldera formation on Earth [e.g., *Branney*, 1995; *Troll et al.*, 2000; *Roche et al.*, 2001; *Holohan et al.*, 2009] suggests that magma chamber evacuation and collapse can occur even in young volcanoes, and so we place the start of the caldera complex's formation early in Ascraeus Mons' history. While the manner and duration of terrace development remains unknown, they are restricted to the main shield, indicating that however long the terraces took to form, they followed the initial shield-building phase, but preceded the construction of the rift aprons. This interpretation can be extended to the arcuate grabens, such that activity along those fractures on the surrounding plains occurred after the rift aprons were emplaced, and that on the flanks followed the late-stage resurfacing event.

[79] We thus propose a time-stratigraphic sequence for the feature types surveyed here that considers the order in which we currently understand Ascraeus Mons to have formed, described in section 2: building of the main shield, followed by the rift aprons, and then by late-stage resurfacing by Amazonian lavas [*Crumpler and Aubele*, 1978; *Bleacher et al.*, 2007a; *Hiesinger et al.*, 2007]. We find that, of the six feature types surveyed, three formed during or after the building of the main shield, and three developed after the late-stage resurfacing event. Specifically, the caldera complex, flank terraces, and small vents were the earliest structures to form, in parallel to or after the main shield, but preceding the construction of the rift aprons. After emplacement of the aprons and subsequent resurfacing, the plains' arcuate grabens formed, followed by the sinuous rilles and pit craters (or at least the last populations thereof). This sequence is illustrated in Figure 11, and is described in detail below.

5.2.1. Initial Shield Building

[80] The length of time taken to develop the main Ascraeus shield is a function of both the effusion rates of shield-building lavas, which may have varied over time [*Plescia*, 2004; *Hiesinger et al.*, 2007], and the nature of this volcanism, which may have been episodic and subject to long periods of repose [*Wilson et al.*, 2001]. It is therefore difficult to estimate with any accuracy how long the initial shield building lasted.

[81] Initial volcanism, its location perhaps influenced by the northeast trending Tharsis structural pattern [*Carr et al.*, 1977], was manifest as accumulations of thick lava plains [*Crumpler and Aubele*, 1978]. Central shield volcano construction followed with the emplacement of basaltic lavas, probably erupted from the summit and sourced from a major magma storage system beneath the volcano.

[82] Following the establishment of an intrusive igneous complex below a nascent Ascraeus Mons, a period of caldera collapse occurred, due to magma chamber inflation and deflation and/or through intrusive loading [*Williams and McBirney*, 1964; *Walker*, 1988; *McBirney*, 1990; *Crumpler et al.*, 1996; *Troll et al.*, 2002] (Figure 11a). Collapse structures formed first to the northwest and southeast (and possibly to the northeast) of the summit plateau; a larger, later collapse then linked these calderas in an elliptical fracture zone oriented southwest-northeast.

[83] Caldera collapse was accommodated by outward-dipping reverse faults [cf. *Branney*, 1995] (Figure 11a, inset: 1), which then acted as magma conduits for subsequent eruptions. With continued volcanism, the edifice was mantled by tephra, lavas, and aeolian sediment, in parallel to mechanical fracturing and hydrothermal alteration due to intrusive activity [cf. *Donoghue et al.*, 2008]. These processes introduced less cohesive strata into the edifice and led to the weakening of progressively buried units (e.g., Figure 5a: 5 and Figure 11a: 2), phenomena commonly observed at Terran volcanoes [*van Wyk de Vries and Francis*, 1997; *van Wyk de Vries et al.*, 2000].

[84] At some point during the growth phase of the volcano, its weight exceeded the yield strength of the supporting basement, which began to flex (Figure 11b). This may

simply have been a viscoelastic response of the supporting lithosphere to the weight of the developing volcano. Alternatively, pressure- and thermal melting could have caused an ice-saturated crust to weaken and bend to the volcanic load [*Murray et al.*, 2010]. Both processes could even have operated together, though the timescale over which each was active is unclear.

[85] During flexure, the volcano entered a state of stress described by *van Wyk de Vries and Matela* [1998], with σ_1 radial, σ_2 concentric, and σ_3 vertical. The radial and concentric constrictional strain at its upper surface was accommodated by a system of inward-dipping, arcuate reverse fault sets [*McGovern and Solomon*, 1993] (Figure 11b: 1), topped by outward-verging thrust folds [*Byrne et al.*, 2009], effectively hanging wall anticlines and manifest as flank terraces (Figure 11b: 2). As flexure induced a "dipole" stress state within the volcano, with extension at its base and compression toward its summit [*McGovern*, 2007;

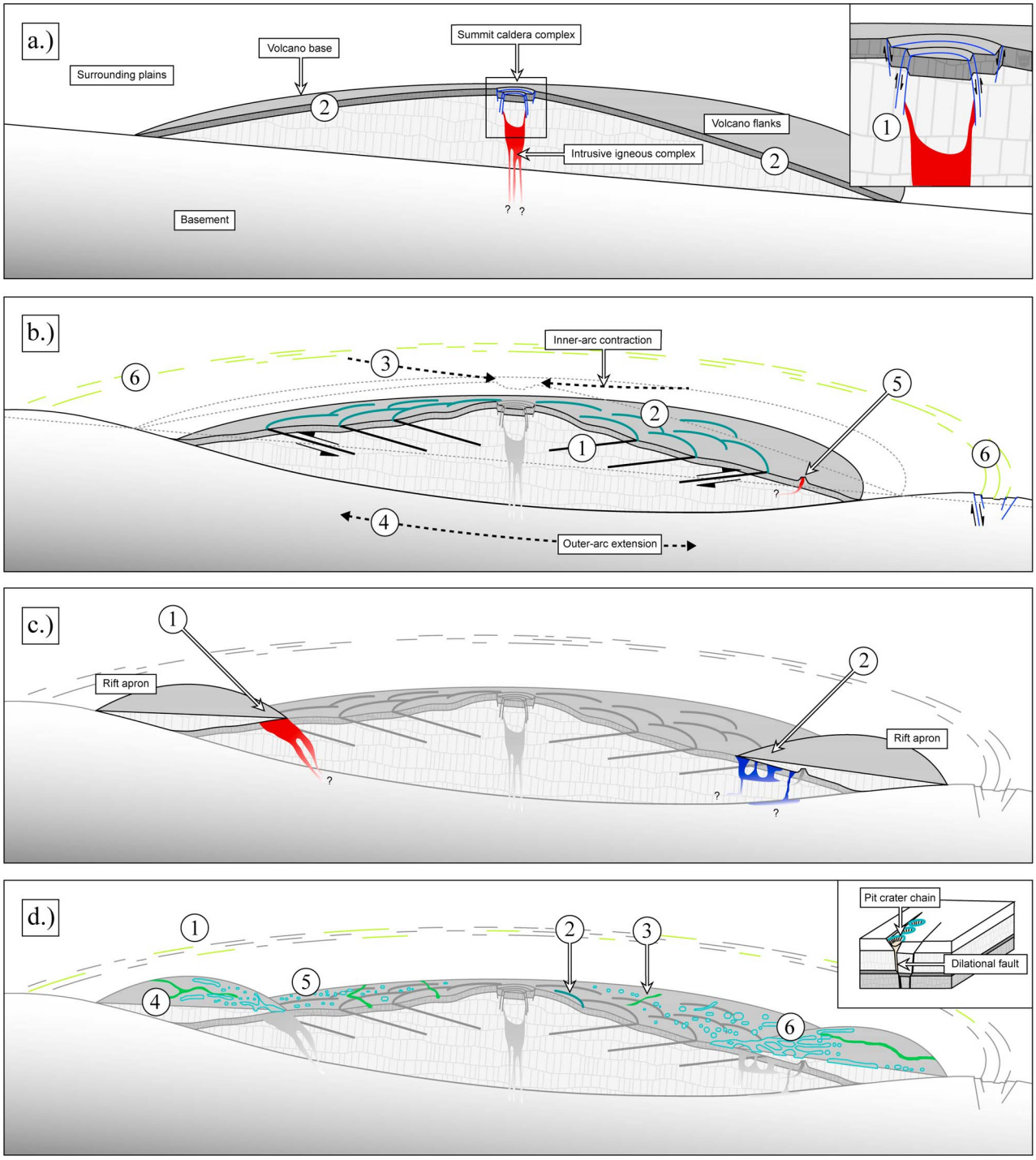

Figure 11

McGovern and Morgan, 2009] (Figure 11b: 3, 4), it is possible that the caldera-bounding fractures were squeezed shut, at least temporarily limiting subsequent collapse.

[86] The terrace bounding faults may have heavily fractured the volcano, extending through its brittle upper strata toward the neutral surface in the edifice. If these shear fractures penetrated into the intrusive core, they may have acted as magma conduits even when actively accommodating flank compression [*Mathieu and van Wyk de Vries*, 2009]. There is little evidence that lavas were sourced from terrace bounding faults or other lineaments on the flanks, however [*Mouginis-Mark*, 1981; *Mouginis-Mark and Christensen*, 2005; *Bleacher et al.*, 2007a], and none of the small flank vents is located on a terrace boundary. Nonetheless, at some time during the main shield-building stage, discrete instances of flank volcanism resulted in the development of small parasitic constructs (Figure 11b: 5), at least on the eastern half of the volcano.

[87] Elastic plate theory predicts that a flexural bulge will form concentric to, and at greater radial distances from, the load [*Comer et al.*, 1985; *Engelder*, 1993; *McGovern and Solomon*, 1993; *Williams and Zuber*, 1995]. This would have resulted in an annular zone of extension about Ascraeus, apparent as a population of shallow, arcuate grabens encircling the volcano (Figure 11b: 6). Initial fractures would have been subsumed by subsequent growth of the edifice. If these structures were subsequently reactivated during extension, however, they could account for the concentric grabens on the volcano's flanks.

5.2.2. Rift Apron Construction

[88] The second major volcanological event to occur at Ascraeus Mons was the formation of the rift aprons to the northeast and southwest (Figure 11c). Although apron construction may have occurred during the main shield-building phase [*Crumpler and Aubele*, 1978], the bulk of the aprons' volume was probably erupted after the development of the main flanks was complete, and may have even followed a considerable period of repose [*Bleacher et al.*, 2007a].

[89] Such a hiatus between main flank and rift apron volcanism could reflect the end of one temporally discrete magma production event and the start of another (Figure 11c: 1), which followed already established magma ascension pathways beneath the Tharsis Montes [*Bleacher et al.*, 2007a]. The location of rift apron activity, at the northeast and southwest base of Ascraeus, was almost certainly influenced by the regional topography of, and subsurface structures throughout, the Tharsis Rise [*Carr et al.*, 1977; *Wilson and Head*, 2002]. The latter included a low-viscosity zone beneath the volcano that acted as a pathway for magmatic ascent and emplacement [*Wilson et al.*, 2001]. This shift in activity could also be partly due to the need for magma to establish new routes to the surface, if previous conduits within the volcano had been closed by upper-flank compression.

[90] Water might also have played a role in shaping the volcano at this time. If at least some rift apron flows were mudflows and lahars [*Murray et al.*, 2010], they may have been sourced from ice-rich layers in the crust beneath Ascraeus, as well as water stored within its flanks [*Scott and Wilson*, 1999; *Mouginis-Mark and Christensen*, 2005] (Figure 11c: 2). Additionally, the late Amazonian-aged fan-shaped deposits extending from the northwest flank show evidence of volcano-ice interaction [*Parsons and Head*, 2005; *Kadish et al.*, 2008]. The proximal ridged terrain on the northwest flanks could also have formed as deposits from water-rich sediment rapidly released from inside the volcano [*Morris et al.*, 2003]. If Ascraeus hosted significant hydrous activity at this time, it would indicate that for some time a set of hydrologically favorable climatic conditions prevailed, which further supports the presence of liquid water at or near the surface of Mars [cf. *Clifford*, 1993; *Mustard et al.*, 2001; *Murray et al.*, 2005; *McCubbin et al.*, 2010].

5.2.3. Late-Stage Amazonian Resurfacing

[91] The latest wide-scale volcanism on Ascraeus Mons occurred during the late Amazonian [*Plescia and Saunders*, 1979], potentially as part of a large magmatic upwelling that resurfaced Arsia and Pavonis Montes, too [*Bleacher et al.*, 2007a] (Figure 11d). These lavas were primarily sourced from the summit, mantling any structures downslope and

Figure 11. Oblique-angle cartoon sequence illustrating the geological history of Ascraeus Mons, through a cross-section of the volcano. (a) Following the construction of a central shield, the evacuation of magma chambers below the edifice led to multiple instances of overburden collapse along outward-dipping reverse faults (shown as (1) and enlarged in the inset), producing a series of summit calderas. Changes in rheology of successively deeper strata may have developed a lithological contrast within the volcano (2). (b) Ensuing flexure of the supporting basement applied a constrictional strain to Ascraeus' upper surface, resulting in a set of inward-dipping fractures (1) topped by hanging wall anticlines (2). A flexurally induced "dipole" stress state saw the volcano experience inner-arc contraction (3) and outer-arc extension (4). Discrete instances of flank volcanism produced parasitic cones on the shield's flanks (5), while extensional fractures formed along the hinge curve of a flexural bulge around the volcano (6). (c) After an eruptive hiatus, new sites of activity on the shield's lower flanks formed expansive, low-angle rift aprons. These constructs could reflect later pulses of magma following existing ascension pathways beneath the Tharsis Montes (1). Water sourced from within or beneath the volcano may also have contributed material to the aprons (2). (d) Extensive resurfacing by Late Amazonian lavas occurred amid continuing flexure, which formed further arcuate grabens on the plains surrounding Ascraeus (1), and the thrust system high on the south flank (2). Sinuous rille formation followed, incising channels upon both the main shield (3) and the rift aprons (4). A final stage of flank tectonism, this time extensional in nature, produced a population of pit craters, crater chains, and troughs across the volcano and its aprons. (A model for dilational faulting along extensional fractures, discussed in section 5.1.3, is shown in the inset, modified from *Wyrick et al.* [2004].) Coalescence of pit chains and troughs eventually formed extensive vermiform embayments on the northeast and southwest flanks (6). Note that neither Ascraeus Mons nor its surface features are to scale in this sequence, nor are their dimensions accurately represented. Each feature type is shown with the color scheme established in Figure 4.

possibly rounding terrace morphology to form the landscape that is currently observed, while partially eroding/covering the few parasitic cones that previously formed on the flanks. Although the total volume of material deposited during this eruptive sequence remains unknown, it was insufficient to bury completely the flank terraces formed up to that point.

[92] Extensional tectonic activity in and around the complex post-dated any summit volcanism, and truncated the most recent lavas to be erupted. The last instances, then, of caldera collapse occurred either due to the withdrawal of magma from a central reservoir and its emplacement elsewhere (within or upon the volcano) [*Mouginis-Mark*, 1981], or due to continued collapse and subsidence because of structural instability in the complex but without attendant large-scale volcanic activity [*Walker*, 1975].

[93] Flexure continued until at least this point in the volcano's history, either as a continuous process or in phases, in the latter case perhaps reinitiating with the addition of the late-stage lavas on the main shield. Load-concentric arcuate grabens formed once again on the plains surrounding the now-established shield (Figure 11d: 1), e.g., toward the northeast of the volcano. Upper flank compression continued after mid-flank volcanism ceased, resulting in the formation of the south flank thrust proximal to the summit (Figures 6b and 11d: 2).

[94] Sinuous rille formation ensued after the end of the resurfacing event, both upon the main flanks and the rift aprons (Figure 11d: 3, 4). Meandering and braided channels were incised into the last Amazonian units to be emplaced, potentially controlled in places by tectonic lineaments within the volcano. If rilles formed due to volcanic erosive [*Cameron*, 1964] or collapse processes [*Greeley*, 1971], then rille formation is likely to have been the last phase of surface volcanism on Ascraeus Mons, with some of this activity originating on the summit. An origin due to erosion by groundwater escaping form the lower flanks [*Murray et al.*, 2010], however, would indicate that subsurface water existed below, and was free to migrate through, the volcano at this point in its history.

[95] The final stage of volcanotectonic deformation on Ascraeus (other than continued minor extension about the caldera complex that fractured proximal sinuous rilles) saw an extensional stress applied to the upper surface of Ascraeus. This resulted in the development of fractures within the edifice with near-circumferential orientations on the main flanks and near-radial along the rift apron axes. Faulting and fracturing along these structures created voids into which overlying material slumped and collapsed, forming thousands of discrete pit crater structures (Figure 11d: 5, inset), with a tendency toward crater chains on the main flanks, and pit troughs on the rift aprons and surrounding plains. Existing planes of weakness within the volcano, such as the fracture zones surrounding each terrace, or older flexure-induced grabens now within its radius, may also have been exploited during this extensional phase. Subsequent erosion and collapse expanded the footprint of these structures, forming coalesced networks of pit troughs to the northeast and southwest of the main shield (Figure 11d: 6).

[96] There is no clear evidence as to why there was a change in the state of stress within the volcano at this point. If the pit craters are the superficial expressions of a dike swarm injected into the edifice, it would mean a further and yet unrecognized period of volcanism on Ascraeus Mons, a volcano that previously experienced pervasive main-shield compressive stresses. Moreover, as previously noted, no flows appear to have originated from the pits. *Montési* [2000] suggested that the plains lavas surrounding Pavonis Mons may have buried its lower flanks while the central part of the volcano remained free, thereby applying a tensional stress to its upper surface. Similar plains lavas encircle Ascraeus, so this process may be equally relevant there.

[97] Alternatively, the volcano's position atop a topographic ridge may have induced a southeast-northwest tensional stress across its upper surface, accounting for the greatest concentration of extensional features along a southwest-northeast axis. This effect could be considered a form of flank spreading, though notably there is no indication of the characteristic "leaf grabens" associated with volcanoes known to be spreading [*Borgia*, 1994; *Merle and Borgia*, 1996]. If this process is responsible for pit crater formation, however, its resultant tensional stress may have existed for as long as has the topography surrounding Ascraeus, expressed only when the flexural response was exhausted, but without further evidence, this possibility remains conjecture.

[98] The final volcanic units to develop within the Ascraeus Mons system were fields of low shields and their associated products distal to the apron margins [*Bleacher et al.*, 2007a; *Hughes et al.*, 2008; *Baratoux et al.*, 2009; *Hauber et al.*, 2009]. Emplaced along existing ascension pathways, this late and low-volume volcanism reflected the waning supply beneath the Tharsis Montes as the late Amazonian magmatic event came to an end.

5.3. Applicability Beyond Ascraeus Mons

[99] This geological history is based upon observations of Ascraeus Mons alone, but may be applicable to volcanoes across Mars. Ascraeus is morphologically similar to the other two Tharsis shields, Arsia and Pavonis Montes [*Carr et al.*, 1977; *Plescia*, 2004], and shares with them a range of superficial structures, including northeast trending rift aprons, concentric grabens, northwest flank aureole deposits, summit calderas, pit crater structures, and imbricate flank terraces [*Crumpler and Aubele*, 1978; *Comer et al.*, 1985; *Hodges and Moore*, 1994; *Crumpler et al.*, 1996; *Wyrick et al.*, 2004; *Byrne et al.*, 2009]. This structural similarity led *Crumpler and Aubele* [1978] to propose the same developmental sequence for all three Tharsis Montes. It should be noted, however, that while these authors regarded Ascraeus as being the least structurally evolved of the three, this volcano shares the same gross structural features as the other Montes, differing from them only in morphometry and age [*Neukum and Hiller*, 1981; *Hodges and Moore*, 1994; *Plescia*, 2004; *Bleacher et al.*, 2007a].

[100] On the basis of their structural similarity, therefore, we suggest that the processes that have shaped Ascraeus Mons contrast to those of Arsia and Pavonis only in terms of duration and extent, but are otherwise equally applicable. We suggest that the other Montes also experienced a main shield-building phase during which caldera collapse and terracing due to flexure occurred, followed by an eruptive hiatus and the eventual formation of extensive rift aprons to the northeast and southwest. Ultimately, a period of flank

extension took place, resulting in the development of prominent grabens and pits across their upper surfaces.

[101] It may even be possible that volcanoes beyond the Tharsis Montes share a similar developmental pattern. For example, a main shield-building phase and periods of caldera collapse appear common to all Martian volcanoes [*Crumpler et al.*, 1996; *Plescia*, 2004; *Williams et al.*, 2009], and many feature pit craters [*Wyrick et al.*, 2004] and flank terraces [*Byrne et al.*, 2009]. Therefore, while the tectonic and magmatic development of a given volcano may differ in detail from that of Ascraeus Mons, the history we propose here establishes a framework with which to approach the volcanotectonic development of a range of volcanoes across Mars.

6. Conclusions

[102] The strength of a multifeature study is that it can provide a holistic framework for understanding geological systems. We have used this approach here to integrate the prominent surface features of Ascraeus Mons into a comprehensive geological history of the volcano, which may in turn be applicable to others across Mars.

[103] Of the six feature types we surveyed on the volcano, we find that three formed relatively early in the volcano's development, concurrent with or after the building of the main shield. The first feature type to develop was the summit caldera complex, followed by the onset of basement flexure and the formation of imbricate terraces on the volcano's flanks. Small parasitic vents across the volcano were also active during this time.

[104] The formation of the latter three feature types was preceded by the construction of the rift aprons and Late Amazonian magmatic activity. Continued flexure led to arcuate grabens crosscutting the resurfaced plains surrounding Ascraeus, while the flanks were hewn with a fluid agent to produce numerous sinuous rilles. The final feature type to form was a prominent population of pit craters and troughs, the result of a late phase of extension across the volcano and its rift aprons.

[105] In an effort to integrate recent terrace mapping results [*Byrne et al.*, 2009] into the existing developmental model of Ascraeus Mons, we have focused primarily where terraces occur, i.e., the volcano's main shield, and have not examined the full extent of the rift aprons. Other recent studies have examined the shield and aprons together, but only along narrow tracts or discrete images [*Mouginis-Mark and Christensen*, 2005; *Bleacher et al.*, 2007a; *Hiesinger et al.*, 2007]. Scope exists, therefore, for expanding this survey to the entire volcanological extent of Ascraeus Mons, to the other Tharsis Montes, and to the other large shields on Mars, especially with the ever-increasing availability of high-resolution photogeological data for the volcanoes of the Red Planet.

[106] **Acknowledgments.** The authors wish to thank the HRSC Experiment Teams at DLR Berlin and the Freie Universität Berlin for their successful planning of the HRSC mission, and for the acquisition, processing, and distribution of HRSC data. We are also grateful to Malin Space Science Systems for the availability of CTX images for use in this work. M. Balme of the Earth and Environmental Sciences Department, The Open University, is thanked for his processing of the CTX images used herein, as well as for his insightful comments on an earlier version of this manuscript. J. Walsh and E. Holohan of the Fault Analysis Group, University College Dublin, and A. O'Halloran, Trinity College Dublin, are thanked for constructive discussion during the preparation of this manuscript. J. Bleacher and an anonymous reviewer are thanked for their help in improving this manuscript. P.K.B. and V.R.T. acknowledge funding from the Department of Geology, Trinity College Dublin, and the Enterprise Ireland International Collaboration program (grant IC/2006/37/A-113). The thesis of P.K.B. is a Co-tutelle agreement between Trinity College Dublin and Université Blaise-Pascal. This research has made use of NASA's Planetary Data System and Astrophysics Data System. The final stages of manuscript preparation were supported by the NASA Planetary Geology and Geophysics Program under grant NNX11AC62G.

References

Baratoux, D., P. Pinet, M. Toplis, N. Mangold, R. Greeley, and A. Baptista (2009), Shape, rheology and emplacement times of small Martian shield volcanoes, *J. Volcanol. Geotherm. Res.*, *185*, 47–68, doi:10.1016/j.jvolgeores.2009.05.003.

Bleacher, J., and R. Greeley (2008), Relating volcano morphology to the developmental progression of Hawaiian shield volcanoes through slope and hypsometric analyses of SRTM data, *J. Geophys. Res.*, *113*, B09208, doi:10.1029/2006JB004661.

Bleacher, J., R. Greeley, D. Williams, S. Cave, and G. Neukum (2007a), Trends in effusive style at the Tharsis Montes, Mars, and implications for the development of the Tharsis province, *J. Geophys. Res.*, *112*, E09005, doi:10.1029/2006JE002873.

Bleacher, J., R. Greeley, D. Williams, S. Werner, E. Hauber, and G. Neukum (2007b), Olympus Mons, Mars: Inferred changes in late Amazonian aged effusive activity from lava flow mapping of Mars Express High Resolution Stereo Camera data, *J. Geophys. Res.*, *112*, E04003, doi:10.1029/2006JE002826.

Bleacher, J., L. Glaze, R. Greeley, E. Hauber, S. Baloga, S. Sakimoto, D. Williams, and T. Glotch (2009), Spatial and alignment analyses for a field of small volcanic vents south of Pavonis Mons and implications for the Tharsis province, Mars, *J. Volcanol. Geotherm. Res.*, *185*, 96–102, doi:10.1016/j.jvolgeores.2009.04.008.

Bleacher, J., A. de Wet, W. Garry, J. Zimbelman, and M. Trumble (2010), Volcanic or fluvial: Comparison of an Ascraeus Mons, Mars, braided and sinuous channel with features of the 1859 Mauna Loa flow and Mare Imbrium flows, *Lunar Planet. Sci.*, *XLI*, Abstract 1612.

Borgia, A. (1994), Dynamic basis of volcanic spreading, *J. Geophys. Res.*, *99*, 17,791–17,804, doi:10.1029/94JB00578.

Borgia, A., and B. van Wyk de Vries (2003), The volcano-tectonic evolution of Concepción, Nicaragua, *Bull. Volcanol.*, *65*, 248–266, doi:10.1007/s00445-002-0256-8.

Branney, M. (1995), Downsag and extension at calderas: New perspectives on collapse geometries from ice-melt, mining, and volcanic subsidence, *Bull. Volcanol.*, *57*, 303–318.

Byrne, P., J. Murray, B. van Wyk de Vries, and V. Troll (2007), Flank terrace architecture of Martian shield volcanoes, *Lunar Planet. Sci.*, *XXXVIII*, Abstract 2380.

Byrne, P., B. van Wyk de Vries, J. Murray, and V. Troll (2009), The geometry of volcano flank terraces on Mars, *Earth Planet. Sci. Lett.*, *281*, 1–13, doi:10.1016/j.epsl.2009.01.043.

Cameron, W. (1964), An interpretation of Schröter's Valley and other lunar sinuous rills, *J. Geophys. Res.*, *69*, 2423–2430.

Carr, M., R. Greeley, K. Blasius, J. Guest, and J. Murray (1977), Some Martian volcanic features as viewed from the Viking orbiters, *J. Geophys. Res.*, *82*, 3985–4015.

Carter, A., B. van Wyk de Vries, K. Kelfoun, P. Bechelèry, and P. Briole (2007), Pits, rifts and slumps: The summit structure of Piton de la Fournaise, *Bull. Volcanol.*, *69*, 741–756, doi:10.1007/s00445-006-0103-4.

Cecchi, E., B. van Wyk de Vries, and J.-M. Lavest (2004), Flank spreading and collapse of weak-cored volcanoes, *Bull. Volcanol.*, *67*, 72–91, doi:10.1007/s00445-004-0369-3.

Chen, L., J. Bleacher, and P. Lowman (2008), The sinuosity of Lunar rilles in the Aristarchus Plateau, *Lunar Planet. Sci.*, *XXXIX*, Abstract 1713.

Cipa, A., J. Bébien, and B. Bonin (1996), Les terrasses et l'escarpement basal du volcan Martien Olympus Mons: Des témoins de vastes glissements gravitaires des flancs?, *C. R. Acad. Sci., Ser. II*, *322*, 369–376.

Clarke, H., V. Troll, and J.-C. Carracedo (2009), Phreatomagmatic to Strombolian eruptive activity of basaltic cinder cones: Montaña Los Erales, Tenerife, Canary Islands, *J. Volcanol. Geotherm. Res.*, *180*, 225–245, doi:10.1016/j.jvolgeores.2008.11.014.

Clifford, S. (1993), The role of the geothermal gradient in the emplacement and replenishment of ground ice on Mars, *Lunar Planet. Sci.*, *XXIV*, Abstract 313.

Comer, R., S. Solomon, and J. Head (1985), Mars: Thickness of the lithosphere from the tectonic response to volcanic loads, *Rev. Geophys.*, *23*, 61–92, doi:10.1029/RG023i001p00061.

Crumpler, L., and J. Aubele (1978), Structural evolution of Arsia Mons, Pavonis Mons and Ascraeus Mons: Tharsis region of Mars, *Icarus*, *34*, 496–511, doi:10.1016/0019-1035(78)90041-6.

Crumpler, L., J. Head, and J. Aubele (1996), Calderas on Mars: Characteristics, structure and associated flank deformation, *Geol. Soc. Spec. Publ.*, *110*, 307–348.

Donoghue, E., V. Troll, C. Harris, A. O'Halloran, J. Perez-Torado, and T. Walter (2008), Low-temperature hydrothermal alteration of intracaldera tuffs, Tejeda caldera, Gran Canaria: Mineralogical and isotopic changes, *J. Volcanol. Geotherm. Res.*, *176*, 551–564, doi:10.1016/j.jvolgeores.2008.05.002.

Engelder, T. (1993), *Stress Regimes in the Lithosphere*, 475 pp., Princeton Univ. Press, Princeton, N. J.

Francis, P., and G. Wadge (1983), The Olympus Mons aureole: Formation by gravitational spreading, *J. Geophys. Res.*, *88*, 333–338, 344.

Geshi, N., T. Shimano, T. Chibam, and S. Nakada (2002), Caldera collapse during the 2000 eruption of Miyakejima Volcano, Japan, *Bull. Volcanol.*, *64*, 55–68, doi:10.1007/s00445-001-0184-z.

Gornitz, V. (1973), The origin of sinuous rilles, *Moon*, *6*, 337–356, doi:10.1007/BF00562210.

Greeley, R. (1971), Lunar Hadley Rille: Considerations of its origin, *Science*, *172*, 722–725, doi:10.1126/science.172.3984.722.

Harris, S. (1977) The aureole of Olympus Mons, Mars, *J. Geophys. Res.*, *82*, 3099–3107.

Harrison, K., and R. Grimm (2005), Groundwater-controlled valley networks and the decline of surface runoff on early Mars, *J. Geophys. Res.*, *110*, E12S16, doi:10.1029/2005JE002455.

Hauber, E., J. E. Bleacher, K. Gwinner, D. Williams, and R. Greeley (2009), The topography and morphology of low shields and associated landforms of plains volcanism in the Tharsis region of Mars, *J. Volcanol. Geotherm. Res.*, *185*, 69–95, doi:10.1016/j.jvolgeores.2009.04.015.

Head, J., and L. Wilson (1998), Tharsis Montes as composite volcanoes?: 1. The role of explosive volcanism in edifice construction and implications for the volatile contents of edifice-forming magmas, *Lunar Planet. Sci.*, *XXIX*, Abstract 1127.

Hiesinger, H., J. Head, and G. Neukum (2007), Young lava flows on the eastern flank of Ascraeus Mons: Rheological properties derived from High Resolution Stereo Camera (HRSC) images and Mars Orbiter Laser Altimeter (MOLA) data, *J. Geophys. Res.*, *112*, E05011, doi:10.1029/2006JE002717.

Hodges, C., and H. Moore (1979) The subglacial birth of Olympus Mons and its aureoles, *J. Geophys. Res.*, *84*, 8061–8074.

Hodges, C., and H. Moore (1994), Atlas of volcanic landforms on Mars, *U.S. Geol. Surv. Prof. Pap.*, *1534*, 194 pp.

Holohan, E., V. Troll, T. Walter, S. Münn, S. McDonnell, and Z. Shipton (2005), Elliptical calderas in active tectonic settings: An experimental approach, *J. Volcanol. Geotherm. Res.*, *144*, 119–136, doi:10.1016/j.jvolgeores.2004.11.020.

Holohan, E., B. van Wyk de Vries, and V. Troll (2008), Analogue models of caldera collapse in strike-slip tectonic regimes, *Bull. Volcanol.*, *70*, 773–796.

Holohan, E., V. Troll, M. Errington, C. Donaldson, G. Nicoll, and C. Emeleus (2009), The Southern Mountains Zone, Isle of Rum, Scotland: Volcanic and sedimentary processes upon an uplifted and subsided magma chamber roof, *Geol. Mag.*, *146*, 400–418, doi:10.1017/S0016756808005876.

Hughes, S., S. Sakimoto, and T. Gregg (2008), A petrogenetic model of plains-style low shield volcanoes on Mars: Implications for magma production in the Tharsis region, *Lunar Planet. Sci.*, *XXXIX*, Abstract 1619.

Hulme, G. (1973), Turbulent lava flow and the formation of lunar sinuous rilles, *Mod. Geol.*, *4*, 107–117.

Irwin, R., A. Howard, and R. Craddock (2006), Theater-headed valleys: The roles of overland flow and groundwater sapping, *Lunar Planet. Sci.*, *XXXVII*, Abstract 1912.

Kadish, S., J. Head, R. Parsons, and D. Marchant (2008), The Ascraeus Mons fan-shaped deposit: Volcano–ice interactions and the climatic implications of cold-based tropical mountain glaciation, *Icarus*, *197*, 84–109, doi:10.1016/j.icarus.2008.03.019.

Laity, J., and M. Malin (1985), Sapping processes and the development of theater-headed valley networks in the Colorado Plateau, *Geol. Soc. Am. Bull.*, *96*, 203–217, doi:10.1130/0016-7606(1985)96<203:SPATDO>2.0.CO;2.

Liu, S., and L. Wilson (1998), Collapse pits due to gas release from shallow dikes on Mars, *Lunar Planet. Sci.*, *XXIX*, Abstract 1602.

Lopes, R., J. Guest, and C. Wilson (1980), Origin of the Olympus Mons Aureole and Perimeter Scarp, *Moon Planets*, *22*, 221–234, doi:10.1007/BF00898433.

Malin, M., et al. (2007), Context Camera investigation on board the Mars Reconnaissance Orbiter, *J. Geophys. Res.*, *112*, E05S04, doi:10.1029/2006JE002808.

Marti, J., G. Ablay, L. Redshaw, and R. Sparks (1994), Experimental studies of collapse calderas, *J. Geol. Soc.*, *151*, 919–929.

Mathieu, L., and B. van Wyk de Vries (2009), Edifice and substrata deformation induced by intrusive complexes and gravitational loading in the Mull volcano (Scotland), *Bull. Volcanol.*, *71*, 1133–1148, doi:10.1007/s00445-009-0295-5.

McBirney, A. (1990), A historical note on the origin of calderas, *J. Volcanol. Geotherm. Res.*, *42*, 303–306, doi:10.1016/0377-0273(90)90006-2.

McCubbin, F., A. Smirnov, H. Nekvasil, J. Wang, E. Hauri, and D. Lindsley (2010), Hydrous magmatism on Mars: A source of water for the surface and subsurface during the Amazonian, *Earth Planet. Sci. Lett.*, *292*, 132–138, doi:10.1016/j.epsl.2010.01.028.

McGovern, P. (2007), Flexural stresses beneath Hawaii: Implications for the October 15, 2006, earthquakes and magma ascent, *Geophys. Res. Lett.*, *34*, L23305, doi:10.1029/2007GL031305.

McGovern, P., and J. Morgan (2005), Spreading of the Olympus Mons volcanic edifice, Mars, *Lunar Planet. Sci.*, *XXXVI*, Abstract 2258.

McGovern, P., and J. Morgan (2009), Volcanic spreading and lateral variations in the structure of Olympus Mons, *Mars, Geology*, *37*, 139–142, doi:10.1130/G25180A.1.

McGovern, P., and S. Solomon (1993), State of stress, faulting, and eruption characteristics of large volcanoes on Mars, *J. Geophys. Res.*, *98*, 23,553–23,579, doi:10.1029/93JE03093.

McGovern, P., S. Solomon, D. Smith, M. Zuber, M. Simons, M. Wieczorek, R. Phillips, G. Neumann, O. Aharonson, and J. Head (2004), Correction to: Localized gravity/topography admittance and correlation spectra on Mars: Implications for regional and global evolution, *J. Geophys. Res.*, *109*, E07007, doi:10.1029/2004JE002286.

Mège, D., and P. Masson (1996), A plume tectonics model for the Tharsis province, Mars, *Planet. Space Sci.*, *44*, 1499–1546.

Merle, O., and A. Borgia (1996), Scaled experiments of volcanic spreading, *J. Geophys. Res.*, *101*, 13,805–13,817, doi:10.1029/95JB03736.

Montési, L. (2000), Concentric dike swarms on the flanks of Pavonis Mons: Implications for the evolution of Martian shield volcanoes and mantle plumes, *Geol. Soc. Spec. Publ.*, *352*, 165–181.

Morgan, J., and P. McGovern (2005), Discrete element simulations of gravitational volcanic deformation: 1. Deformation structures and geometries, *J. Geophys. Res.*, *110*, B05402, doi:10.1029/2004JB003252.

Morris, A., P. Mouginis-Mark, and S. Baloga (2003), Did glaciers exist recently on the Tharsis Montes?, *EOS Trans. AGU*, *84*(46), Fall Meet. Suppl., Abstract P32C-08.

Morris, E. (1982), Aureole deposits of the Martian volcano Olympus Mons, *J. Geophys. Res.*, *87*, 1164–1178.

Mouginis-Mark, P. (1981), Late-stage summit activity of Martian shield volcanoes, *Proc. Lunar Planet. Sci. Conf.*, *12th*, 1431–1447.

Mouginis-Mark, P. (2003), New observations of the diversity of eruption styles along the SW rift zone of Arsia Mons, Mars, Abstract 3001 presented at the Sixth International Conference on Mars, Calif. Inst. of Technol., Pasadena, Calif., 20–25 July.

Mouginis-Mark, P., and P. Christensen (2005), New observations of volcanic features on Mars from the THEMIS instrument, *J. Geophys. Res.*, *110*, E08007, doi:10.1029/2005JE002421.

Mouginis-Mark, P., and S. Rowland (2008), Lava flows at Arsia Mons, Mars: Insights from a graben imaged by HiRISE, *Icarus*, *198*, 27–36, doi:10.1016/j.icarus.2008.06.015.

Mouginis-Mark, P., L. Wilson, J. Head, S. Brown, J. Hall, and K. Sullivan (1984), Elysium Planitia, Mars: Regional geology, volcanology, and evidence for volcano-ground ice interactions, *Earth Moon Planets*, *30*, 149–173, doi:10.1007/BF00114309.

Murray, J., et al. (2005), Evidence from the Mars Express High Resolution Stereo Camera for a frozen sea close to Mars' equator, *Nature*, *434*, 352–356, doi:10.1038/nature03379.

Murray, J., B. van Wyk de Vries, A. Marquez, D. Williams, P. Byrne, J.-P. Muller, and J.-R. Kim (2010), Late-stage water eruptions from Ascraeus Mons volcano, Mars: Implications for its structure and history, *Earth Planet. Sci. Lett.*, *294*, 479–491, doi:10.1016/j.epsl.2009.06.020.

Mustard, J., C. Cooper, and M. Rifkin (2001), Evidence for recent climate change on Mars from the identification of youthful near-surface ground ice, *Nature*, *412*, 411–414, doi:10.1038/35086515.

Neukum, G., and K. Hiller (1981), Martian ages, *J. Geophys. Res.*, *86*, 3097–3121.

Neukum, G., et al. (2004), Recent and episodic volcanic and glacial activity on Mars revealed by the High Resolution Stereo Camera, *Nature*, *432*, 971–979, doi:10.1038/nature03231.

Oehler, J.-F., B. van Wyk de Vries, and P. Labazuy (2005), Landslides and spreading of oceanic hot-spot and arc shield volcanoes on Low Strength

Layers (LSLs): An analogue modeling approach, *J. Volcanol. Geotherm. Res.*, *144*, 169–189, doi:10.1016/j.jvolgeores.2004.11.023.
Parsons, R., and J. Head (2005), Ascraeus Mons fan-shaped deposit, Mars: Geological history and volcano-ice interactions of a cold-based glacier, *Lunar Planet. Sci.*, *XXXVI*, Abstract 1139.
Peale, S., G. Schubert, and R. Lingenfelter (1968), Distribution of sinuous rilles and water on the Moon, *Nature*, *220*, 1222–1225.
Plescia, J. (2004), Morphometric properties of Martian volcanoes, *J. Geophys. Res.*, *109*, E03003, doi:10.1029/2002JE002031.
Plescia, J., and R. Saunders (1979), The chronology of the Martian volcanoes, *Proc. Lunar Planet. Sci. Conf.*, *10th*, 2841–2859.
Robbins, S., G. Di Achille, and B. Hynek (2011), The volcanic history of Mars: High-resolution crater-based studies of the calderas of 20 volcanoes, *Icarus*, *211*, 1179–1203, doi:10.1016/j.icarus.2010.11.012.
Roche, O., B. van Wyk de Vries, and T. Druitt (2001), Sub-surface structures and collapse mechanisms of summit pit craters, *J. Volcanol. Geotherm. Res.*, *105*, 1–18, doi:10.1016/S0377-0273(00)00248-1.
Rowland, S., and H. Garbeil (2000), Slopes of oceanic basalt volcanoes, in *Remote Sensing of Active Volcanism*, *Geophys. Monogr. Ser*, vol. 116, edited by P. J. Mouginis-Mark et al., pp. 223–247, AGU, Washington, D. C., doi:10.1029/GM116p0223.
Rymer, H., B. van Wyk de Vries, J. Stix, and G. Williams-Jones (1998), Pit crater structure and processes governing persistent activity at Masaya Volcano, Nicaragua, *Bull. Volcanol.*, *59*, 345–355, doi:10.1007/s004450050196.
Schultz, R., and M. Zuber (1994), Observations, models, and mechanisms of failure of surface rocks surrounding planetary surface loads, *J. Geophys. Res.*, *99*, 14,691–14,702, doi:10.1029/94JE01140.
Scott, D., and K. Tanaka (1986), Geologic map of the western equatorial region of Mars, *U. S. Geol. Surv. Misc. Invest. Ser. Map*, *I-1802-A*.
Scott, D., G. Schaber, and K. Tanaka (1981), Map showing lava flows in the southeast part of the Tharsis quadrangle of Mars, *Map I-1269*, U.S. Geol. Surv, Reston, Va.
Scott, E., and L. Wilson (1999), Evidence for a sill emplacement event on the upper flanks of the Ascraeus Mons shield volcano, Mars, *J. Geophys. Res.*, *104*, 27,079–27,089, doi:10.1029/1999JE001049.
Scott, E., and L. Wilson (2000), Cyclical summit collapse events at Ascraeus Mons, Mars, *J. Geol. Soc. London*, *157*, 1101–1106.
Scott, E., L. Wilson, and J. Head (2000), Martian plinian eruptions and pit chain craters, *Lunar Planet. Sci.*, *XXXI*, Abstract 1332.
Smith, D., et al. (2001), Mars Orbiter Laser Altimeter: Experiment summary after the first year of global mapping of Mars, *J. Geophys. Res.*, *106*, 23,689–23,722, doi:10.1029/2000JE001364.
Spencer, J., and F. Fanale (1990), New models for the origin of Valles Marineris closed depressions, *J. Geophys. Res.*, *95*, 14,301–14,313, doi:10.1029/JB095iB09p14301.
Tanaka, K. (1985), Ice-lubricated gravity spreading of the Olympus Mons aureole deposits, *Icarus*, *62*, 191–206, doi:10.1016/0019-1035(85)90117-4.
Tanaka, K., and M. Golombek (1989), Martian tension fractures and the formation of grabens and collapse features at Valles Marineris, *Proc. Lunar Planet. Sci. Conf.*, *19th*, 383–396.
Thomas, P., S. Squyres, and M. Carr (1990), Flank tectonics of Martian volcanoes, *J. Geophys. Res.*, *95*, 14,345–14,355, doi:10.1029/JB095iB09p14345.
Thurber, C., and M. Toksöz (1978), Martian lithospheric thickness from elastic flexure theory, *Geophys. Res. Lett.*, *5*, 977–980, doi:10.1029/GL005i011p00977.
Troll, V., C. Emeleus, and C. Donaldson (2000), Caldera formation in the Rum Igneous Complex, Scotland, *Bull. Volcanol.*, *62*, 301–317, doi:10.1007/s004450000099.
Troll, V., T. Walter, and H.-U. Schmincke (2002), Cyclic caldera collapse: Piston or piecemeal subsidence? Field and experimental evidence, *Geology*, *30*, 135–138, doi:10.1130/0091-7613(2002)030<0135:CCCPOP>2.0.CO;2.
van Wyk de Vries, B., and A. Borgia (1996), The role of basement in volcano deformation, *Geol. Soc. Spec. Publ.*, *110*, 95–110.
van Wyk de Vries, B., and P. Francis (1997), Catastrophic collapse at stratovolcanoes induced by gradual volcano spreading, *Nature*, *387*, 387–390, doi:10.1038/387387a0.
van Wyk de Vries, B., and R. Matela (1998), Styles of volcano-induced deformation: Numerical models of substratum flexure, spreading and extrusion, *J. Volcanol. Geotherm. Res.*, *81*, 1–18, doi:10.1016/S0377-0273(97)00076-0.
van Wyk de Vries, B., N. Kerle, and D. Petley (2000), Sector collapse forming at Casita volcano, Nicaragua, *Geology*, *28*, 167, doi:10.1130/0091-7613(2000)28<167:SCFACV>2.0.CO;2.
Walker, G. (1975), A new concept of the evolution of the British Tertiary intrusive centres, *J. Geol. Soc.*, *131*, 121–141, doi:10.1144/gsjgs.131.2.0121.
Walker, G. (1988), Three Hawaiian calderas: Origin through loading by shallow intrusion?, *J. Geophys. Res.*, *93*, 14,773–14,784, doi:10.1029/JB093iB12p14773.
Walter, T., and V. Troll (2001), Formation of caldera periphery faults: An experimental study, *Bull. Volcanol.*, *63*, 191–203, doi:10.1007/s004450100135.
Werner, S. (2009), The global Martian volcanic evolutionary history, *Icarus*, *201*, 44–68, doi:10.1016/j.icarus.2008.12.019.
Williams, D., R. Kerr, and C. Lesher (1998), Emplacement and erosion by Archean komatiite lava flows at Kambalda: Revisited, *J. Geophys. Res.*, *103*, 27,533–27,549, doi:10.1029/97JB03538.
Williams, D., R. Greeley, E. Hauber, K. Gwinner, and G. Neukum (2005), Erosion by flowing Martian lava: New insights for Hecates Tholus from Mars Express and MER data, *J. Geophys. Res.*, *110*, E05006, doi:10.1029/2004JE002377.
Williams, D., et al. (2009), The Circum-Hellas Volcanic Province, Mars: Overview, *Planet. Space. Sci.*, *57*, 895–916.
Williams, H., and A. McBirney (1964), Petrologic and structural contrast of the quaternary volcanoes of Guatemala, *Bull. Volcanol.*, *27*, 61–67.
Williams, K., and M. Zuber (1995), An experimental study of incremental surface loading of an elastic plate: Application to volcano tectonics, *Geophys. Res. Lett.*, *22*, 1981–1984.
Wilson, L., and J. Head (1994), Mars: review and analysis of volcanic eruption theory and relationships to observed landforms, *Rev. Geophys.*, *32*, 221–263.
Wilson, L., and J. Head (2002), Tharsis-radial graben systems as the surface manifestation of plume-related dike intrusion complexes: Models and implications, *J. Geophys. Res.*, *107*(E8), 5057, doi:10.1029/2001JE001593.
Wilson, L., E. Scott, and J. Head (2001), Evidence for episodicity in the magma supply to the large Tharsis volcanoes, *J. Geophys. Res.*, *106*, 1423–1433.
Wolfe, E., W. Wise, and G. Dalrymple (1997), The geology and petrology of Mauna Kea Volcano, Hawaii: A study of postshield volcanism, *U.S. Geol. Surv. Prof. Pap.*, *1557*, 129 pp.
Wyrick, D., D. Ferrill, A. Morris, S. Colton, and D. Sims (2004), Distribution, morphology, and origins of Martian pit crater chains, *J. Geophys. Res.*, *109*, E06005, doi:10.1029/2004JE002240.
Zimbelman, J., and K. Edgett (1992), The Tharsis Montes, Mars: Comparison of volcanic and modified landforms, *Proc. Lunar Planet. Sci. Conf.*, *22nd*, 31–44.
Zimbelman, J., and R. McAllister (1985), Surface morphology on the Martian volcano Ascraeus Mons, *Proc. Lunar Planet. Sci. Conf.*, *16th*, 936–937.
Zuber, M., and P. Mouginis-Mark (1992), Caldera subsidence and magma chamber depth of the Olympus Mons volcano, Mars, *J. Geophys. Res.*, *97*, 18,295–18,307.
Zuber, M., D. Smith, S. Solomon, D. Muhleman, J. Head, J. Garvin, J. Abshire, and J. Bufton (1992), The Mars Observer laser altimeter investigation, *J. Geophys. Res.*, *97*, 781–787, 797.

P. K. Byrne, Department of Terrestrial Magnetism, Carnegie Institution of Washington, 5241 Broad Branch Rd. NW, Washington, DC 20015–1305, USA. (pbyrne@dtm.ciw.edu)
J. B. Murray, Department of Earth Sciences, Open University, Milton Keynes MK7 6AA, UK.
V. R. Troll, Department of Earth Sciences, Uppsala University, SE-752 36 Uppsala, Sweden.
B. van Wyk de Vries, Laboratoire Magmas et Volcans, Université Blaise-Pascal, F-63038 Clermont-Ferrand, France.